A Synthetic Approach Reveals Extensive Tunability of Auxin Signaling[1][C][W][OA]

Kyle A. Havens[2], Jessica M. Guseman[2], Seunghee S. Jang[2], Edith Pierre-Jerome[2], Nick Bolten, Eric Klavins, and Jennifer L. Nemhauser*

Department of Electrical Engineering (K.A.H., S.S.J., N.B., E.K.), and Department of Biology (J.M.G., E.P.J., J.L.N.), University of Washington, Seattle, Washington 98195

Explaining how the small molecule auxin triggers diverse yet specific responses is a long-standing challenge in plant biology. An essential step in auxin response is the degradation of Auxin/Indole-3-Acetic Acid (Aux/IAA, referred to hereafter as IAA) repressor proteins through interaction with auxin receptors. To systematically characterize diversity in degradation behaviors among IAA | receptor pairs, we engineered auxin-induced degradation of plant IAA proteins in yeast (*Saccharomyces cerevisiae*). We found that IAA degradation dynamics vary widely, depending on which receptor is present, and are not encoded solely by the degron-containing domain II. To facilitate this and future studies, we identified a mathematical model able to quantitatively describe IAA degradation behavior in a single parameter. Together, our results demonstrate the remarkable tunability conferred by specific configurations of the auxin response pathway.

Auxin directs almost every aspect of plant biology, yet how specificity is generated from auxin signaling components remains largely unresolved. A range of auxin-associated phenotypes, including profound disruptions in development and severely compromised responses to environmental signals, are caused by single amino acid substitutions that stabilize transcriptional corepressor proteins called the Auxin/Indole-3-Acetic Acids (Aux/IAAs, referred to hereafter as IAAs; Chapman and Estelle, 2009). The diversity of these phenotypes and the size of the IAA family suggest that IAAs may provide specificity in auxin responses (Lokerse and Weijers, 2009). Functional studies support this idea, as stabilized IAAs provoke different phenotypes even when expressed from the same promoter (Weijers et al., 2005; Muto et al., 2007).

Auxin activates gene expression by enhancing IAA turnover through interaction with auxin receptors, a family of F-box proteins called TRANSPORT INHIBITOR RESISTANT1 (TIR1)/AUXIN SIGNALING F-BOX PROTEINS (AFBs; Dharmasiri et al., 2005a; Kepinski and Leyser, 2005), referred to here collectively as AFBs. Variation in the affinities of IAA | AFB pairs has recently been observed (Calderón Villalobos et al., 2012). How such differences relate to degradation kinetics is still unclear. Labor-intensive seedling studies on a small number of IAA proteins, in combination with analysis of stabilized IAA mutants, uncovered the importance of a conserved region, termed domain II, in determining protein stability. The degron-containing IAA domain II is both necessary and sufficient for interaction with TIR1 and the resulting auxin-induced degradation (Ramos et al., 2001; Dharmasiri et al., 2005a; Kepinski and Leyser, 2005; Tan et al., 2007). In addition, IAA-reporter fusions with diverse domain II sequences show a range of degradation rates when overexpressed in Arabidopsis (*Arabidopsis thaliana*) seedlings (Dreher et al., 2006). However, the ubiquity of the auxin pathway in plants and the difficulty in reconstituting the complete degradation machinery in vitro have hindered further characterization of the molecular determinants of IAA degradation rates.

As a complement to existing systems and to systematically characterize the potential tunability of different IAA | AFB pairs, we engineered the auxin-induced degradation of IAA proteins in the yeast *Saccharomyces cerevisiae*. Our synthetic system has several advantages: precise control of auxin input levels, the ability to study IAA | AFB pairs in isolation, and the absence of the many other plant pathways known to impact auxin signaling (Stewart and Nemhauser, 2010). Our system allowed a comprehensive survey of

[1] This work was supported by the Paul G. Allen Family Foundation and the National Science Foundation (grant nos. CISE–0832773 to E.K. and IOS–0919021 to J.L.N.). J.M.G. was supported by the National Institutes of Health (training grant no. T32HD007183). E.P.J. was supported by a National Science Foundation Graduate Research Fellowship and the Seattle Chapter of the Achievement Rewards for College Scientists Foundation.

[2] These authors contributed equally to the article.

* Corresponding author; e-mail jn7@uw.edu.

The author responsible for distribution of materials integral to the findings presented in this article in accordance with the policy described in the Instructions for Authors (www.plantphysiol.org) is: Jennifer L. Nemhauser (jn7@uw.edu).

[C] Some figures in this article are displayed in color online but in black and white in the print edition.

[W] The online version of this article contains Web-only data.

[OA] Open Access articles can be viewed online without a subscription.

www.plantphysiol.org/cgi/doi/10.1104/pp.112.202184

IAA protein turnover while recapitulating behaviors observed in plants. We discovered that the particular AFB receptor used greatly impacted the rate of degradation and that sequences outside of the degron-containing domain II accelerated or decelerated IAA degradation in an IAA-specific manner. Moreover, we identified a mathematical model that provides a single parameter to quantitatively describe degradation behavior. The synthetic toolkit described here will facilitate rapid testing of hypotheses about the ubiquitylation of IAA proteins and suggests a means to characterize other hormone-induced protein degradation pathways.

RESULTS

A Synthetic Yeast System Recapitulates Auxin-Induced IAA Degradation Dynamics

Our engineered auxin response system consisted of pairwise matings of yeast expressing either yellow fluorescent protein (YFP)-IAA fusion proteins or AFBs (Fig. 1A). In the presence of a functional AFB, YFP fluorescence (a proxy for IAA protein levels) could be both up- and down-regulated by modulating the levels of indole-3-acetic acid, hereafter referred to as auxin (Fig. 1B; Supplemental Fig. S1). The timing and extent of degradation were comparable to experimental systems relying on a much higher concentration of a synthetic auxin (Nishimura et al., 2009). Flow cytometry provided high-resolution IAA degradation profiles for each IAA|AFB pair with improved time-resolution measurements at the single cell level (Fig. 1C). In contrast to the "basal degradation" rates observed in plants (Dreher et al., 2006), YFP-IAA proteins were essentially stable in yeast in the absence of auxin or a functional AFB (Supplemental Figs. S2 and S3). This may reflect the difficulty of completely clearing auxin from plant cells or the presence of additional components in plants that are absent from our synthetic system. Following the major auxin-induced degradation

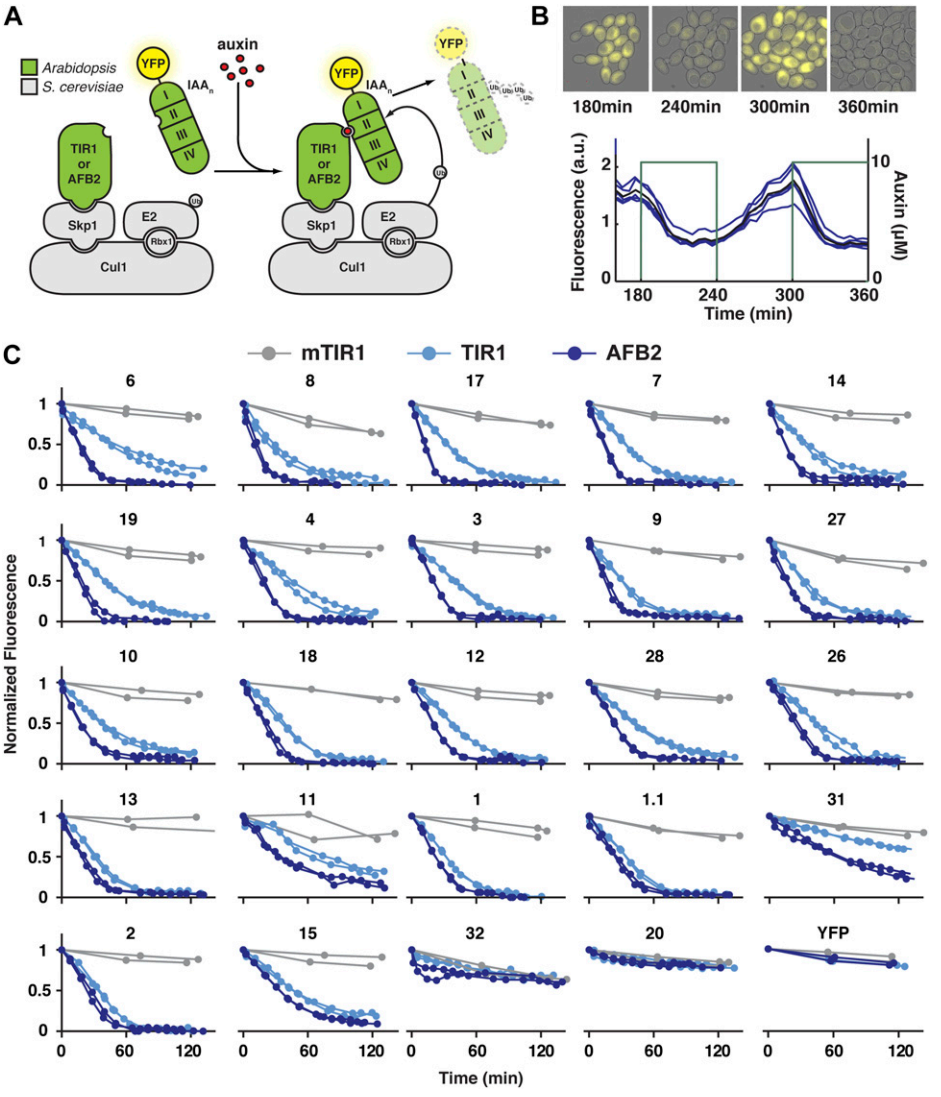

Figure 1. IAA degradation is highly variable. A, Plant auxin receptors (TIR1 or AFB2) and YFP-tagged IAA repressors were integrated into the yeast ubiquitin pathway, shown in gray. B, Yeast cells were imaged while exposed to a square wave of auxin. Auxin leads to a rapid decrease in YFP (fluorescence of individual microcolonies in blue, average value in black), which can be recovered with auxin removal. C, A range of IAA|receptor degradation rates were obtained using time-lapse flow cytometry. Degradation curves were normalized to starting fluorescence. IAAs are listed in order of the relative difference in degradation in the presence of TIR1 versus AFB2. Strains expressing the F-box-deficient mTIR1 show no auxin-dependent degradation. [See online article for color version of this figure.]

events, a more gradual decline in YFP can be observed. As this behavior was also observed in strains expressing mTIR1, we believe that this decrease in fluorescence is caused by physiological changes associated with increasing culture density and not auxin-induced degradation of YFP-IAAs.

The fine time resolution of our measurements resulted in complex degradation profiles that included an initial delay in degradation prior to an exponential decay of YFP levels (Fig. 1, B and C; Supplemental Fig. S9). Standard half-life calculations, therefore, were insufficient to describe the dynamics of degradation in our system. In order to quantitatively characterize the degradation behavior of every IAA | AFB pair, we identified a second-order nonlinear model that captures the dynamic auxin response in both time-course and dose-response experimental data (Fig. 2A; Supplemental File S1; Supplemental Figs. S9–S11; Supplemental Tables S3 and S7). This model accounts for the complex degradation behavior we observed and the nonlinear relationship between auxin concentration and steady-state YFP intensity (Supplemental Fig. S1). Among the candidate models tested, this model had the least complexity while still fitting the data with low residual error (Supplemental File S1). Auxin response is represented by YFP-IAA fluorescence intensity output y and a hypothesized internal state x, dependent on the auxin input concentration u. The hypothesized internal state x is not directly measured in our experiments and does not necessarily equate with specific active species, although one interpretation is that x is a complex formed between auxin and an AFB. Similarly, parameters k_1, k_2, k_3, k_4, and k_5 are not intended to have direct association with physical values in the system. One possibility is that these rates correlate with synthesis (k_1 for the internal state and k_3 for the IAA), degradation of the internal state (k_2), basal degradation/dilution of the IAA (k_4), and AFB-induced degradation (k_5). With this interpretation and applying the principles of global curve fitting, we reduced the total number of parameters needed to fit the entire data set (Supplemental File S1).

Modeling distilled the differences observed in degradation between the IAA | AFB pairs into a single parameter, k_5. Importantly, the k_5 value for each IAA | AFB pair is consistent with the qualitative behaviors present in the experimental data (Figs. 1C and 2C). For example, the faster degrading IAAs had the largest k_5 values, while more stable IAAs had the lowest k_5 values. Of all the parameters, k_5 best captures IAA | AFB degradation behavior and is hereafter called the degradation rate.

IAA Proteins Exhibit a Range of Degradation Rates

In our system, auxin-induced degradation differs across IAA | AFB pairs (Figs. 1C and 2C). This is consistent with previous work in Arabidopsis seedlings, where half-lives of overexpressed IAA-LUC fusions were calculated by blocking new protein production with cycloheximide and treating exogenously with the synthetic auxin 2,4-dichlorophenoxyacetic acid (Dreher et al., 2006; Supplemental Table S1). In these assays, a strong match to the consensus domain II sequence was correlated with a short protein half-life in the presence of 2,4-dichlorophenoxyacetic acid. For example, IAA17 and IAA28 have strong matches to the consensus domain II and half-lives of 5 and 15 min, respectively. In contrast, IAA31, with a diverged domain II, has a half-life of approximately 4 h. IAA20 lacks a recognizable domain II sequence and is highly stable. We observed similar patterns of degradation in yeast (Figs. 1C and 2C). In yeast expressing either TIR1 or AFB2, IAAs with consensus-matching domain II sequences degraded rapidly, IAA31 was slow to degrade, and IAA20

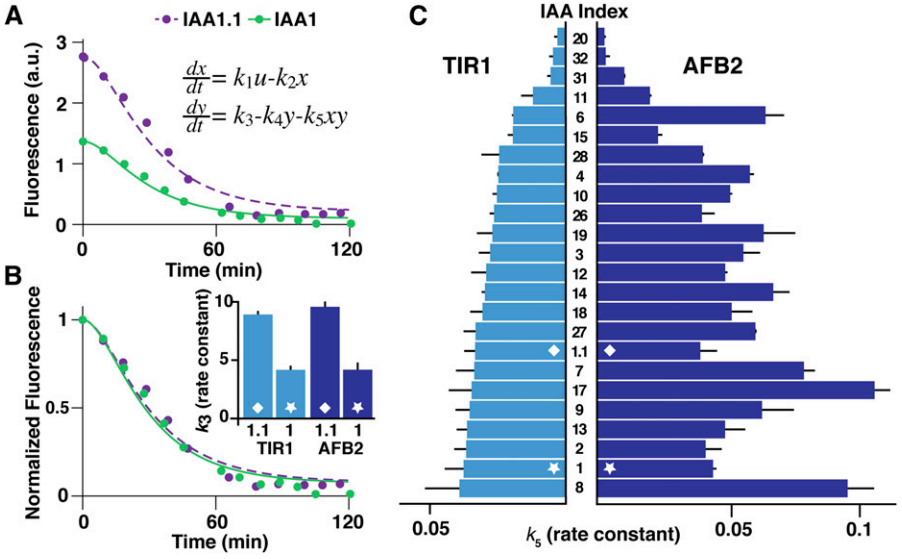

Figure 2. Degradation dynamics can be described using few parameters. A, Our model is described by two ordinary differential equations. Degradation curves for AFB2 strains expressing IAA1 or yeast codon-optimized IAA1.1 are shown. B, k_5 is largely independent of expression levels. IAA1 and IAA1.1 degradation curves overlap after normalization, although there is an approximately 2-fold difference in k_3 values. C, IAA|AFB2 pairs have increased degradation rates (k_5), a different rank order when compared with IAA/TIR1 pairs, and an increased dynamic range between the slowest and fastest pairs. Parameters were estimated for two independent replicates. All error bars represent 1 SD. Additional parameters are listed in Supplemental Tables S4 and S5. a.u., Arbitrary units. [See online article for color version of this figure.]

showed no degradation. Of the IAAs with consensus domain II sequences, most IAA | TIR1 pairs had rates similar to the fast-degrading IAA17 | TIR1 (Fig. 2C). We observed a few IAAs outside of this general trend, including the slow-degrading IAA11.

Despite being expressed from the same promoter and singly integrated in the same genomic location, IAAs displayed different basal fluorescence levels in yeast (Supplemental Fig. S3). Our model predicts that rates of IAA expression and degradation are independent of each other (Supplemental File S1). To test this prediction, we synthesized a variant allele of IAA1 (IAA1.1) with yeast-optimized codons. Basal expression of IAA1.1 was twice that of IAA1 (Fig. 2A), with a similar fold change in the estimated k_3 values (Fig. 2B). In contrast, normalized degradation curves and k_5 values overlapped (Fig. 2, B and C). This result validates our model and demonstrates that IAA degradation rates are indeed robust to fluctuations in IAA expression levels. Challenges in plant assays, including random location of insertions and multiple cell types contributing to variation in transgene expression, make this type of quantitative analysis quite difficult and highlight the benefits of using yeast as an additional resource for dynamic analysis of auxin responses.

IAA Degradation Rates Are Receptor Specific

For the majority of IAAs tested, AFB2 promoted faster degradation than TIR1 (Figs. 1C and 2C). This resulted in IAA | AFB2 pairs having degradation rates up to three times higher than IAA | TIR1 pairs. IAA | AFB2 pairs also had a wider range of degradation rates between all IAAs. Excluding the IAAs with divergent domain IIs, the fastest IAA | TIR1 pair (IAA8) had a degradation rate 3.3-fold higher than the slowest, IAA11. In contrast, the fastest IAA | AFB2 pair (IAA17) had a degradation rate 5.5-fold higher than IAA11. Strikingly, the rank order of degradation rates was not maintained between strains expressing different receptors. IAA6 showed one of the slowest rates of degradation with TIR1, yet it had one of the fastest degradation rates for IAA | AFB2 pairs. A subset of IAAs showed little difference in degradation between auxin receptors, leading to some of the widest discrepancies in relative rank order. For example, there was little or no change in IAA1 degradation when the receptor was switched from TIR1 to AFB2. This resulted in IAA1 being one of the fastest degrading IAAs in combination with TIR1 yet among the slowest when expressed with AFB2. While it is possible that AFB2 functions more efficiently than TIR1 in yeast, the identification of a subset of IAAs that show no change in degradation between the two receptors suggests that these two proteins are intrinsically different in their IAA interactions.

While TIR1 and AFB2 conferred rapid auxin-induced degradation of IAAs, AFB1 and AFB3 had little effect on IAA degradation rates (Supplemental Fig. S4). Genetic analysis suggests that TIR1 and AFB2 are the major auxin receptors in Arabidopsis, but it is still unclear the degree to which each TIR1/AFB protein contributes to specific auxin responses (Dharmasiri et al., 2005b; Parry et al., 2009). Mutations in *TIR1* or *AFB2* lead to stronger overall auxin-related phenotypes than mutations in *AFB1* or *AFB3*, although the loss of *AFB1* or *AFB3* can enhance mutations in other AFB family members (Dharmasiri et al., 2005b; Parry et al., 2009). We reasoned that AFBs might differ in their ability to interact with IAAs. This hypothesis is consistent with our findings as well as with in vitro pull-down assays showing that AFB1 and AFB3 have lower levels of interaction with IAAs than TIR1 and AFB2 (Parry et al., 2009). In addition, IAA-reporter fusions are strongly stabilized in *afb2* mutants, while loss of *AFB1* or *AFB3* alone has little effect on turnover rates (Dharmasiri et al., 2005b). An additional factor may be that our heterologous degradation assay is less sensitive than other assays to weak or transient IAA-AFB interactions. Indeed, in vitro pull-down assays and yeast two-hybrid screens have shown low levels of interaction between some IAA | AFB pairs even in the absence of auxin (Dharmasiri et al., 2005a, 2005b; Kepinski and Leyser, 2005; Parry et al., 2009; Calderón Villalobos et al., 2012), while we did not see any change in IAA stability without auxin addition (Supplemental Figs. S2 and S3). Moreover, auxin can increase interactions between AFB1-DNA-binding domain fusion proteins and IAA-activation domain fusion proteins when both constructs are highly expressed in yeast (Calderón Villalobos et al., 2012), suggesting that these weaker interactions may contribute to auxin responses in plants. Additional work in plants will be needed to discriminate among these different possibilities.

Receptor expression levels did not influence IAA degradation in our yeast assays. Degradation rates were not correlated with receptor abundance (Supplemental Fig. S5), nor could they be increased by adding a second copy of the same receptor to the genome (Supplemental Fig. S6). In addition, when TIR1 and AFB2 were coexpressed, the degradation rate of IAA6 closely matched that of AFB2 alone (Supplemental Fig. S6). Genetic studies indicate that TIR1 is the primary auxin receptor, and AFB2 is not able to substitute for TIR1 even when expressed from the TIR1 promoter (Parry et al., 2009). This suggests that degradation rate differences are not the sole distinguishing characteristic of receptors and that further functional studies of the dynamics of IAA degradation in receptor mutant backgrounds could be fruitful.

Residues Outside of Domain II Differentially Affect Degradation Rates

Residues outside of domain II have been found to contribute to IAA | AFB auxin-binding affinity in vitro (Calderón Villalobos et al., 2012) and high basal IAA

degradation rates in seedlings (Dreher et al., 2006). We engineered truncations in IAAs with disparate degradation rates (Fig. 3A; Supplemental Fig. S7) to directly test the role of nondomain II residues in auxin-induced degradation. The N-terminal half of the protein (T1) or a smaller region restricted to domain II (T2) was fused to an SV40 nuclear localization signal (NLS; Supplemental Table S2). Degradation rates of truncated proteins were compared with full-length constructs fused to the same NLS (Fig. 3, B and C). We found that sequences outside of domain II could accelerate or decelerate degradation rates in an IAA-specific manner. Relative rank order of full-length IAA degradation rates was not conserved in the truncations. IAA28.T2 was the fastest degrading of the T2 truncations, yet IAA28 showed much slower degradation rates than IAA1 or IAA6. Moreover, parallel truncations in different IAAs did not have the same effect on degradation rates. IAA6.T1 was slower than full-length IAA6, but IAA28.T1 was faster than full-length IAA28.

The recently reported DII-VENUS auxin sensor is similar to IAA28.T2 but shifted 15 amino acids toward the IAA28 N terminus (Vernoux et al., 2011; Brunoud et al., 2012). To test whether this small difference in sequence had any effect on degradation rates, we engineered the identical IAA28 truncation into our system (IAA28.T2V; Fig. 3A; Supplemental Table S2). IAA28.T2V degraded far slower than all other constructs tested (Fig. 3B). This effect is opposite to what we observed with IAA28.T1 and IAA28.T2, both of which had increased rates of degradation compared with the full-length protein. The markedly slower degradation rate we observed for IAA28.T2V could explain why it was the brightest reporter tested (Brunoud et al., 2012). In fact, our analysis predicted that IAA8 and IAA9, the other IAA truncations tested in that study, would degrade faster than IAA28 (Fig. 2; Supplemental Table S1). This is consistent with the much dimmer fluorescence observed for the DII reporters made with these IAA proteins (Brunoud et al., 2012). To directly test whether our yeast assays could predict relative degradation rates in plants, we generated transgenic seedlings expressing a modified DII-VENUS reporter where we replaced the IAA28.T2V sequence with the IAA28.T2 sequence. Consistent with the higher rate of turnover of the IAA28.T2 fusion protein in yeast, we observed significantly lower levels of fluorescence of the IAA28.T2 reporter in transgenic plants (Supplemental Fig. S8).

DISCUSSION

The size and diversity of the IAA and AFB protein families suggest that auxin specificity can be conferred by specific configurations of IAA and AFB family members (Lokerse and Weijers, 2009). In this study, we present a new method for investigating the range of diversity encoded by these large families. By porting plant proteins into yeast, we could directly test the variability in degradation rates between specific IAA | AFB pairs. We were able to reproduce auxin-induced degradation and generate high-resolution real-time data. Our yeast platform was able to recapitulate behaviors previously observed in studies of IAA turnover and allowed for an extensive survey of IAA degradation behavior.

Assessing degradation with each receptor individually, we showed that IAA degradation is highly influenced by which receptor is present and that these receptor effects are IAA specific (Figs. 1C and 2C). Our data provide evidence of receptor choice on regulating the turnover of IAAs and show that each

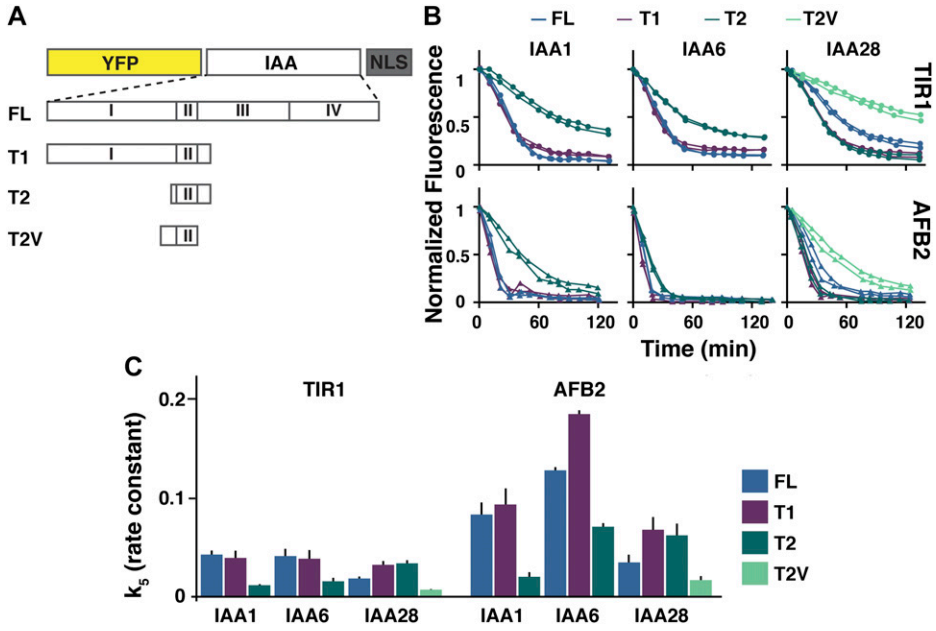

Figure 3. Residues outside of domain II contribute to auxin-induced degradation rates. A, Schematic of IAA truncations. B and C, Degradation dynamics of full-length proteins are not maintained in truncations. B, Degradation rates of truncations expressed with TIR1 or AFB2, normalized to the starting fluorescence for each strain. C, Parameters k_3 and k_5 were determined using parameters k_1, k_2, and k_4 from previous model fitting. Additional parameters are listed in Supplemental Table S6.

member of the IAA | AFB pair plays a role in determining auxin sensitivity. The high sequence similarity between TIR1 and AFB2, in combination with their shared substrates, should provide a platform to dissect how F-box proteins influence the rate of ubiquitylation, a factor known to vary among other F-box proteins (Pierce et al., 2009). The lack of detectable IAA degradation in yeast expressing AFB1 or AFB3, despite their ability to bind auxin, may have important implications for calibrating auxin responses. This implies that different combinations of receptors may produce varied response thresholds, which may each trigger a specific auxin-regulated process (Reinhardt et al., 2003; Del Bianco and Kepinski, 2011).

Surprisingly, IAA degradation rates were not strongly correlated with the few recently reported in vitro dissociation constants (Calderón Villalobos et al., 2012; Supplemental Table S1). This lack of correlation could simply be the result of the artificial nature of both systems: dissociation constants are a measure of complex formation and are determined independent of a complete ubiquitin complex, and our heterologous system has a mixture of yeast and plant components (Fig. 1A). However, a testable alternative hypothesis is that the interaction strength between TIR1 and an IAA is not a direct reflection of how quickly the IAA is degraded. Conserved sequences outside of the interaction domain have recently been shown to impact the rate of degradation of a number of substrates of the anaphase-promoting complex (Williamson et al., 2011). While similar sequences have not been identified in IAA proteins, the fact that truncations have such varied degradation rates clearly shows that additional residues play a crucial role in modulating interaction with the ubiquitin machinery (Fig. 3; Dreher et al., 2006). Identification of IAA degradation rate determinants could be accelerated by combining information from studies in yeast, in vitro, and in plants.

By utilizing a small, data-driven model, we were able to quantitatively characterize the complex degradation behavior of each IAA | AFB pair in response to auxin (Fig. 2). Mathematical modeling allowed us to distinguish IAA and AFB contributions to degradation and thereby demonstrate how auxin perception can be tuned. We chose a small, empirical model because large mechanistic models (Bridge et al., 2012) require more parameters than could be identified from the low-dimensional output available in our experiments. Small models can nevertheless be quite useful. For example, a new negative feedback loop was discovered in yeast osmoadaptation using a small-model approach (Mettetal et al., 2008). Similarly, our simple model showed that unknown molecular interactions beyond complex affinity are required to describe IAA degradation dynamics. Moreover, small models such as ours can provide a simple description of the input-output properties of a module and facilitate the rational design of new systems in synthetic biology.

In this study, we have demonstrated the utility of porting a pathway to an orthogonal organism to characterize its function. As a single-celled eukaryote with conserved cellular machinery, yeast provides a seminatural context that facilitates the study of complex signaling pathways. The rapid generation time, control of insertion site and number, and high-throughput methods for quantitative analysis, combined with the absence of other known confounding factors like auxin transport, auxin metabolism, and the coexpression of AFB and IAA family members, make studies in yeast a strong complement to plant studies. Given the obvious artificiality of our system, it is quite promising that the rank order of auxin-induced degradation rates parallels the limited number of half-lives observed in plants (Supplemental Table S1). The fact that the IAA28.T2 construct behaved as predicted when expressed in seedlings (Fig. 3; Supplemental Fig. S8) also points to overall conservation in degradation determinants between plant cells and engineered yeast. A full analysis of the similarities and differences between the systems will require more plant studies and likely better tools for measuring dynamic behaviors in plants. Our heterologous system provides a new method to investigate auxin signaling as well as suggests a means to study the many other plant pathways that rely on ubiquitin-mediated protein degradation.

MATERIALS AND METHODS

Yeast Methods

Yeast transformations were performed using a standard lithium acetate protocol (Gietz and Woods, 2002) into *MAT*a W303-1A or *MAT*α W814-29B, a gift from the Gottschling laboratory. Yeast Peptone Dextrose (YPD) and Synthetic Complete (SC) medium supplemented with 80 mg mL^{-1} adenine were made according to standard protocols. All strains used in this study are listed in Supplemental Table S9.

Strain Construction

IAAs, TIR1, and AFB were amplified from Arabidopsis (*Arabidopsis thaliana*) complementary DNA (Columbia ecotype) using the primers listed in Supplemental Table S8. A partial attB1 site and Kozak sequence (AAA) were added to the 5′ end of each forward primer (5′-AAAAAGCAGGCTTCAAA-3′), and a partial attB2 site was added to the 5′ end of each reverse primer (5′-AGAAAGCTGGGTG-3′). The remaining attB1 and attB2 sequences were added with a second PCR using generic forward and reverse adapter primers (5′-GGGGACAAGTTTGTACAAAAAAGCAGGCT-3′ and 5′-GGGGACCACTTTGTACAAGAAAGCTGGGT-3′). Products were subcloned into a Gateway pDONR221 plasmid using a standard Gateway BP reaction (BP Clonase II; Life Technologies). Each complementary DNA was fully sequenced and then cloned into destination vectors with a standard Gateway LR reaction (LR Clonase II; Life Technologies). IAAs were cloned into pGP4GY-ccdB (Trp selection), and auxin receptors were cloned into pGP5G-ccdB (Leu selection; K.A. Havens, N. Bolten, J.L. Nemhauser, and E. Klavins, unpublished data). Approximately 300 ng of each plasmid was digested with *Pme*I and transformed: pGP4GY-IAA into W303-1A, pGP5G-AFB into W814-29B. Integrations were confirmed by PCR. Strains to be mated were coinoculated at low density into YPD medium, grown overnight at 30°C, and struck out to single colonies on SC-His-Trp to select for diploids.

IAA truncations were fused to an N-terminal YFP and C-terminal SV40 NLS repeat using Gly-Ala linkers (GAGAGAGAGAGP and GAGA, respectively; Nishimura et al., 2009). The IAA17.T1 construct was synthesized with partial EYFP and the complete NLS sequence (www.genewiz.com) and then cloned into the pGP4GY-ccdB vector backbone via Gibson assembly (Gibson et al., 2009). The cloning scheme is outlined in Supplemental Figure S7.

Primers are listed in Supplemental Table S8. Gateway acceptor sites were removed by this process. Further truncation constructs were amplified from full-length IAA sequences and cloned in place of IAA17 using Gibson assembly (Gibson et al., 2009).

The DII-VENUS plasmid was a gift from Teva Vernoux. The IAA28.T2-VENUS plasmid was constructed by replacing the DII region of DII-VENUS with the IAA28.T2 degron region using Gibson assembly (Gibson et al., 2009).

Flow Cytometry

YFP intensity measurements were taken with a BD Accuri C6 flow cytometer with a CSampler plate adapter using excitation wavelengths of 488 and 640 nm and an emission detection filter at 533 nm (FL1 channel). A total of 10,000 events above a 400,000 FSC-H threshold (to exclude debris) were measured for each sample at a flow rate of 66 μL min^{-1} and core size of 22 μm using the Accuri C6 CFlow Sampler software. Cytometry data were exported as FCS 3.0 files and processed using the flowCore R software package and custom R scripts to obtain the mean FL1-A value at each time point. The script applies two polygon gates on the data to isolate single yeast cells. One gate separates the total yeast population from debris on the SSC-A and FSC-A channels. The second gate isolates single cells from cell aggregates (doublet discrimination) via their higher FSC-H (peak height) to FSC-A (peak area) ratio. Scripts are available upon request.

Degradation Assays

Cells were prepared by transferring a freshly grown colony from YPD plates into SC. The cell density (in events μL^{-1}) was estimated using cytometry data gated for yeast by a custom R script. Each culture was then diluted to 0.5 events μL^{-1} in 15 mL of SC. This dilution was split into duplicate 4-mL aliquots with the exception of controls. For IAA17 without a YFP tag and YFP without an IAA, only a single 4-mL aliquot was prepared. YFP-IAA17 was split into three aliquots to serve as an internal replicate control within each experiment. Aliquots were incubated for 16 h at 30°C with shaking. At 16 h, duplicate aliquots of each strain were mixed and split again into two tubes. Cultures were in log phase at the beginning of each experiment (density measured in the cytometer at approximately 500 events μL^{-1}) and remained in log phase for the duration of each experiment (Supplemental Fig. S2).

Measurements were taken at two time points prior to the addition of any treatment. For each strain, one replicate was mock treated (95% [v/v] ethanol) and one replicate was treated with 10 μM indole-3-acetic acid (the minimal concentration of auxin needed to promote complete IAA degradation during log-phase growth of the yeast; Supplemental Figs. S1 and S2). As soon as possible after the addition of auxin, fluorescence for the 0-min time point was recorded. Subsequent measurements were acquired at 10-min intervals for the first 2 h after auxin addition and every 30 min thereafter until the fluorescence level in most strains had plateaued (approximately 3.5 h). Controls were measured every hour for the duration of the experiment.

Modeling and Quantitative Analysis

Modeling methods and quantitative analysis are described in Supplemental File S1.

Microscopy

Yeast cells grown overnight in SC at 30°C were diluted 1:100 in SC, incubated for 4 to 5 h, and then diluted 1:20 before loading onto a Y04D plate (CellASIC). Using the CellASIC-ONIX microfluidic system and associated software, cells were pulsed with a square wave of 10 μM auxin in SC medium over a period of 2 h. An inverted Nikon Eclipse Ti microscope with a 60×, numerical aperture 1.4 oil objective was used to image the yeast cells at 5-min intervals using a YFP-HYQ 535 bandpass filter (Nikon; excitation at 515 nm, detection from 520 to 550 nm) and a CoolSNAP HQ2 14 bit camera. Image processing was done with custom MATLAB scripts, available upon request. Briefly, a segmentation algorithm was applied to bright-field images to produce a binary mask for each microcolony. This binary mask was then applied to the YFP image to calculate the average YFP intensity value within the colony. Background fluorescence level was estimated using the average fluorescence of a 100- × 100-pixel square away from the yeast colony and subtracted from total fluorescence values.

Generation and Analysis of Transgenic Plants

Columbia ecotype plants were transformed using the floral dip method (Clough and Bent, 1998). T1 plants were selected on 0.5× LS agar plates containing 30 μg mL^{-1} hygromycin B. Plates were stratified for 2 d, exposed to light for 6 h, and then grown in the dark for 3 d following a modification of the method of Harrison et al. (2006). Resistant seedlings were transferred to plates containing no antibiotics and allowed to recover for an additional 3 d. DII-VENUS seeds provided generously by Teva Vernoux were grown in identical conditions to allow a direct comparison of the IAA28.T2 and IAA28.T2V constructs in plants.

Plants were imaged using a Leica DMI 3000B microscope fitted with a Leica long-working 20× HCX PL FLUORTAR objective and illuminated with a Lumencor SOLA light source. Images were captured using Leica LAS AF version 2.6.0 software and a Leica DFC 345FX camera. Seven independent IAA28.T2 transformants were examined and compared with 10 DII-VENUS seedlings. Fiji software was used to quantify fluorescence in a region of interest centered on each image.

Supplemental Data

The following materials are available in the online version of this article.

Supplemental Figure S1. Addition of 10 μM auxin is sufficient for maximal degradation of IAAs.

Supplemental Figure S2. Fluorescence levels decrease drastically as yeast cells enter the stationary phase.

Supplemental Figure S3. AFBs do not have differential effects on basal degradation of IAAs.

Supplemental Figure S4. AFB1 and AFB3 do not promote degradation of IAA2.

Supplemental Figure S5. TIR1 is expressed at a similar level to AFB2.

Supplemental Figure S6. AFB2 expression is not rate limiting.

Supplemental Figure S7. Cloning scheme for domain II truncation constructs.

Supplemental Figure S8. Fluorescence accumulation differs between IAA28 truncations in plants.

Supplemental Figure S9. Sample time-course IAA degradation data and model fits of IAA14|TIR1.

Supplemental Figure S10. Sample dose-response data and model predicted dose response of IAA17|AFB2.

Supplemental Figure S11. Parameter variations study of the preferred model.

Supplemental Table S1. Comparison of degradation rates, half-lives, and affinities from yeast, in vitro, and plant studies.

Supplemental Table S2. Table of amino acids included in each IAA truncation.

Supplemental Table S3. The residuals and the number of distinct parameters for all candidate models.

Supplemental Table S4. Estimated parameters for IAA|TIR1 pairs using the preferred model interpretation.

Supplemental Table S5. Estimated parameters for IAA|AFB2 pairs using the preferred model interpretation.

Supplemental Table S6. Estimated parameters for degron comparison study using the preferred model interpretation.

Supplemental Table S7. Average, minimum, and maximum values of the estimated parameters.

Supplemental Table S8. Oligonucleotides used in this study

Supplemental Table S9. Yeast strains used in this study.

Supplemental File S1. Quantitative Analysis.

ACKNOWLEDGMENTS

We thank Mark Estelle, Ning Zheng, and members of the Nemhauser and Klavins groups for helpful discussions and Alec Nielson, Selma Alkafeef, and Brandi House for technical assistance.

Received June 18, 2012; accepted July 25, 2012; published July 27, 2012.

LITERATURE CITED

Bridge LJ, Mirams GR, Kieffer ML, King JR, Kepinski S (2012) Distinguishing possible mechanisms for auxin-mediated developmental control in Arabidopsis: models with two Aux/IAA and ARF proteins, and two target gene-sets. Math Biosci **235:** 32–44

Brunoud G, Wells DM, Oliva M, Larrieu A, Mirabet V, Burrow AH, Beeckman T, Kepinski S, Traas J, Bennett MJ, et al (2012) A novel sensor to map auxin response and distribution at high spatio-temporal resolution. Nature **482:** 103–106

Calderón Villalobos LI, Lee S, De Oliveira C, Ivetac A, Brandt W, Armitage L, Sheard LB, Tan X, Parry G, Mao H, et al (2012) A combinatorial TIR1/AFB-Aux/IAA co-receptor system for differential sensing of auxin. Nat Chem Biol **8:** 477–485

Chapman EJ, Estelle M (2009) Mechanism of auxin-regulated gene expression in plants. Annu Rev Genet **43:** 265–285

Clough SJ, Bent AF (1998) Floral dip: a simplified method for Agrobacterium-mediated transformation of Arabidopsis thaliana. Plant J **16:** 735–743

Del Bianco M, Kepinski S (2011) Context, specificity, and self-organization in auxin response. Cold Spring Harb Perspect Biol **3:** a001578

Dharmasiri N, Dharmasiri S, Estelle M (2005a) The F-box protein TIR1 is an auxin receptor. Nature **435:** 441–445

Dharmasiri N, Dharmasiri S, Weijers D, Lechner E, Yamada M, Hobbie L, Ehrismann JS, Jürgens G, Estelle M (2005b) Plant development is regulated by a family of auxin receptor F box proteins. Dev Cell **9:** 109–119

Dreher KA, Brown J, Saw RE, Callis J (2006) The *Arabidopsis* Aux/IAA protein family has diversified in degradation and auxin responsiveness. Plant Cell **18:** 699–714

Gibson DG, Young L, Chuang R-Y, Venter JC, Hutchison CA III, Smith HO (2009) Enzymatic assembly of DNA molecules up to several hundred kilobases. Nat Methods **6:** 343–345

Gietz RD, Woods RA (2002) Transformation of yeast by lithium acetate/single-stranded carrier DNA/polyethylene glycol method. Methods Enzymol **350:** 87–96

Harrison SJ, Mott EK, Parsley K, Aspinall S, Gray JC,, Cottage A (2006) A rapid and robust method of identifying transformed Arabidopsis thaliana seedlings following floral dip transformation. Plant Methods **2:** 19

Kepinski S, Leyser O (2005) The Arabidopsis F-box protein TIR1 is an auxin receptor. Nature **435:** 446–451

Lokerse AS, Weijers D (2009) Auxin enters the matrix: assembly of response machineries for specific outputs. Curr Opin Plant Biol **12:** 520–526

Mettetal JT, Muzzey D, Gómez-Uribe C, van Oudenaarden A (2008) The frequency dependence of osmo-adaptation in Saccharomyces cerevisiae. Science **319:** 482–484

Muto H, Watahiki MK, Nakamoto D, Kinjo M, Yamamoto KT (2007) Specificity and similarity of functions of the *Aux/IAA* genes in auxin signaling of Arabidopsis revealed by promoter-exchange experiments among *MSG2/IAA19*, *AXR2/IAA7*, and *SLR/IAA14*. Plant Physiol **144:** 187–196

Nishimura K, Fukagawa T, Takisawa H, Kakimoto T, Kanemaki M (2009) An auxin-based degron system for the rapid depletion of proteins in nonplant cells. Nat Methods **6:** 917–922

Parry G, Calderon-Villalobos LI, Prigge M, Peret B, Dharmasiri S, Itoh H, Lechner E, Gray WM, Bennett M, Estelle M (2009) Complex regulation of the TIR1/AFB family of auxin receptors. Proc Natl Acad Sci USA **106:** 22540–22545

Pierce NW, Kleiger G, Shan SO, Deshaies RJ (2009) Detection of sequential polyubiquitylation on a millisecond timescale. Nature **462:** 615–619

Ramos JA, Zenser N, Leyser O, Callis J (2001) Rapid degradation of auxin/indoleacetic acid proteins requires conserved amino acids of domain II and is proteasome dependent. Plant Cell **13:** 2349–2360

Reinhardt D, Pesce E-R, Stieger P, Mandel T, Baltensperger K, Bennett M, Traas J, Friml J, Kuhlemeier C (2003) Regulation of phyllotaxis by polar auxin transport. Nature **426:** 255–260

Stewart JL, Nemhauser JL (2010) Do trees grow on money? Auxin as the currency of the cellular economy. Cold Spring Harb Perspect Biol **2:** a001420

Tan X, Calderon-Villalobos LI, Sharon M, Zheng C, Robinson CV, Estelle M, Zheng N (2007) Mechanism of auxin perception by the TIR1 ubiquitin ligase. Nature **446:** 640–645

Vernoux T, Brunoud G, Farcot E, Morin V, Van den Daele H, Legrand J, Oliva M, Das P, Larrieu A, Wells D, et al (2011) The auxin signalling network translates dynamic input into robust patterning at the shoot apex. Mol Syst Biol **7:** 508

Weijers D, Benkova E, Jäger KE, Schlereth A, Hamann T, Kientz M, Wilmoth JC, Reed JW, Jürgens G (2005) Developmental specificity of auxin response by pairs of ARF and Aux/IAA transcriptional regulators. EMBO J **24:** 1874–1885

Williamson A, Banerjee S, Zhu X, Philipp I, Iavarone AT, Rape M (2011) Regulation of ubiquitin chain initiation to control the timing of substrate degradation. Mol Cell **42:** 744–757

Supplementary Information for

A synthetic approach reveals extensive tunability of auxin signaling

Kyle A. Havens[1*], Jessica M. Guseman[2*], Seunghee S. Jang[1*], Edith Pierre-Jerome[2*], Nick Bolten[1], Eric Klavins[1#], and Jennifer L. Nemhauser[2#]

[1]Department of Electrical Engineering
[2]Department of Biology
University of Washington, Seattle, WA, 98195
[*]co-first authors
[#]correspondence should be addressed to klavins@uw.edu or jn7@uw.edu

Contents

Supplementary Figures

Supplementary Tables

1 Quantitative Analysis

1.1 Objectives and Approach

The primary objective of our quantitative analysis is to identify a small model, with as few parameters as possible, that describes the differential degradation of IAA|AFB pairs observed in experiments. Having few parameters avoids over-fitting, facilitates comparison among available pairs, and provides a guide for the selection of parts during the rational design of new networks. A computationally intractable number of candidate models can be generated by, for example, various assumptions about the mechanism of degradation and the many molecular species involved. Computational limits, therefore, require that we limit the number of candidate models by employing current knowledge of the auxin signal pathway, basic assumptions about protein synthesis, and simple input-output concepts.

We assess candidate models by fitting their parameters to the entire data set, analyzing their qualitative fit, and then computing their residual fit. We fit our models to experimental data using the nonlinear optimization function `FindFit` in *Mathematica* (Wolfram) where the cost function is defined as

$$J(\theta^{(s)}, M_s) \;=\; \sum_{i,j} \sum_{t_m \in \mathrm{T}} \left\| y_{ij}(t_m) - \hat{y}_{ij}(t_m, \theta_{ij}^{(s)}, M_s) \right\|_2 , \tag{1}$$

where i denotes the index of an IAA, j denotes the index of a AFB, s denotes the index of a model, $y_{ij}(t_m)$ denotes the measured output at $t = t_m$, T denotes the set of measurement times, $\theta_{ij}^{(s)}$ denotes the parameter vector for a model M_s and $\mathrm{IAA}_i|\mathrm{AFB}_j$, $\hat{y}_{ij}(t_m, \theta_{ij}, M_s)$ denotes the predicted output using the model M_s and its parameter vector θ_{ij} at $t = t_m$, $\theta^{(s)}$ denotes the union of all parameter vectors of IAA|AFB pairs under the model M_s and $\|\cdot\|_2$ denotes the 2-norm[1] of the given vector. Following the estimation, the residual of a model is defined as

$$G(M_s) = \sum_{i,j} \sum_{t_m \in \mathrm{T}} \frac{1}{dim\ y_{ij}} \left\| \frac{y_{ij}(t_m) - \hat{y}_{ij}\left(t_m, M_s, \theta_{ij}^{(s)*}\right)}{y_{ij}(t_m)} \right\|_2 \tag{2}$$

where $\theta^{(s)*}$ denotes the optimal estimated parameter vector obtained from minimizing the cost function (1), and *dim* denotes the dimension of the vector (e.g. number of data points in the time course).

1.2 Model Development and Discrimination

Our approach is to develop candidate models with good qualitative fits, low residuals, and a small number of parameters by incrementally increasing complexity via refinements that are based on known mechanisms. In the model discrimination step, both quantitative and qualitative metrics of each model are evaluated. It is true that quantitatively low residual is desired in general, however, the analytical metric takes precedence. If a model is shown to be analytically incapable of fitting critical features of experimental observation, the model is deemed structurally flawed, and is eliminated, even if the quantitative metric is relatively low. Following are the two general qualitative features observed in the experimental data.

[1] $\|x\|_p = \left(\sum_{i=1}^{n} |x_i|^p\right)^{1/p}$

1. Each degradation time-course includes an inflection point, such that the curve switches from concave to convex (Figure 1C).

2. Each dose-response curve (steady-state fluorescence measurement vs auxin concentration) is nonlinear (Supplementary Figure 1).

These two features were used as qualitative criteria to which all models were subjected to. The number of parameters for the model is computed over all experimental data sets, such that the total number of parameters equals the number of parameters in the model multiplied by the number of experiments (i.e. the number of distinct IAA|AFB pairs). After a model has been selected, we reduced the total number of parameters by assuming that some of the parameters can be consolidated for a specific group of experiments.

1.2.1 M_0

We first consider the synthetic yeast system as a grey-box with a single input (auxin) and a single output (YFP intensity). Therefore, we propose the following model, M_0, which is a combination of simple synthesis/degradation dynamics and exponential decay:

$$\frac{d\,y(t)}{dt} = k_1 - k_2\,y(t) - k_3\,u(t)\,y(t), \tag{3}$$

where t denotes time, y denotes the output, and u denotes the input. This model encodes the hypothesis that the YFP-IAA fusion protein is subject to zeroth-order synthesis and first-order degradation, and that the output degrades at a rate proportional to the input. The first two terms, k_1 and $k_2\,y(t)$, represent the input-independent synthesis and degradation of the output, respectively. The last term represents the degradation of output with the overall rate proportional to itself and the input. Thus, k_1 is the synthesis rate, k_2 is the basal degradation rate, and k_3 is the input mediated degradation rate.

This model has residual $G(M_0) = 49.31$, and requires 144 distinct parameters (3 per IAA|AFB pair) to fit the entire data set. The model has a closed form analytical solution,

$$y(t) \;=\; \frac{k_1}{k_2 + k_3 u}\left(1 + \frac{e^{-t(k_2+k_3u)}k_3 u}{k_2}\right), \tag{4}$$

which demonstrates the nonlinear relationship between u and the y^*, which is consistent with the qualitative observation of the experimental data (Supplementary Figure 9, purple curve). However, the model cannot capture the inflection of the curve (Supplementary Figure 9, purple curve). For a function to have change in its convexity, the second derivative has to equal zero at some $t > 0$ (and that t is the inflection point). However, M_0 has second-order derivative,

$$\frac{d^2y}{dt^2} \;=\; \frac{k_1 k_3 u\,(k_2 + k_3 u)}{k_2} e^{-t(k_2+k_3u)} \tag{5}$$

which shows that for all parameters $k_1, k_2, k_3 > 0$ and $u \geq 0$, $d^2y/dt^2 > 0$. This represents M_0 is fundamentally unable to capture one of the crucial features of the system.

1.2.2 M_1

The inflection point and the related initial delay in the degradation curves suggest that the IAA degradation mechanism comprises additional intermediate processes (e.g. formation of an intermediate species). To model this feature, we add an internal state x. At this point, we do not assume that x is any specific species or combination of species – just that it is formed and degraded. In particular, we assume that the

rate at which x is synthesized is proportional to the input, and that x affects the non-basal degradation of y. This second-order linear model, M_1, is defined by

$$\begin{aligned}\frac{d\,x(t)}{dt} &= k_1\,u(t) - k_2\,x(t)\\ \frac{d\,y(t)}{dt} &= k_3 - k_4\,y(t) - k_5\,x(t).\end{aligned} \tag{6}$$

The model has residual $G(M_1) = 81.68$, and requires 240 distinct parameters (5 per IAA|AFB pair) to fit the entire data set. The model captures the inflection point in time-course degradation curve (Supplementary Figure 9, blue curve). However, the dose-response predicted by M_1 is qualitatively different from our observations. Analytically, the steady-state solution of M_1 has a closed form,

$$\begin{aligned}x^* &= \frac{k_1\,u}{k_2}\\ y^* &= \frac{k_3}{k_4} - \frac{k_5\,k_1}{k_2\,k_4}u,\end{aligned} \tag{7}$$

which demonstrates that y^* has a linear relationship to u. Furthermore, because of this linear relationship, the model predicts that the steady-state fluorescence decreases indiscriminately with increasing amount of input, to the point where negative fluorescence is predicted (Supplementary Figure 10, blue curve). The fact that M_2 makes predictions that starkly contradict physical constraints demonstrates that M_1 is qualitatively unfit for the given experimental data.

1.2.3 M_2

Since the dose-response is nonlinear, we modify M_1 by introducing a nonlinear term, making the degradation term dependent on $y(t)$. This second-order nonlinear model, M_2, is,

$$\begin{aligned}\frac{dx(t)}{dt} &= k_1\,u(t) - k_2\,x(t)\\ \frac{dy(t)}{dt} &= k_3 - k_4\,y(t) - k_5\,x(t)\,y(t),\end{aligned} \tag{8}$$

which has a residual of $G(M_2) = 24.54$ and requires 240 distinct parameters (5 per IAA|AFB pair) to fit the entire data set. The steady-state of output predicted by M_2 are,

$$\begin{aligned}x^* &= \frac{k_1\,u}{k_2}\\ y^* &= \frac{k_2 k_3}{k_2 k_4 + k_1 k_5 u},\end{aligned} \tag{9}$$

which demonstrates a nonlinear relationship between y^* and u, which satisfies one of the qualitative features. There is no closed-form solution for the model because it is nonlinear, however, numerical solution demonstrates that the model captures the inflection point in the predicted time-course curves (Supplementary Figures 9 and 10, green curve).

1.2.4 M_3

As mentioned before, the internal state x represents an unknown intermediate species (or combination of species) that interacts with auxin input and the YFP-IAA output. It is feasible that more than a single intermediate species is required to encompass the underlying dynamics. To investigate whether this might be the case, we added a second internal state, z, as an intermediate state between x and y. This third-order

nonlinear model, M_3, is

$$\begin{aligned}\frac{dx(t)}{dt} &= k_1\,u(t) - k_2\,x(t),\\ \frac{dz(t)}{dt} &= k_3\,x(t) - k_4\,z(t),\\ \frac{dy(t)}{dt} &= k_5 - k_6\,y(t) - k_7\,z(t)\,y(t),\end{aligned} \tag{10}$$

which has a residual of $G(M_3) = 33.30$ and requires 336 distinct parameters (7 parameters per IAA|AFB pair) to fit the entire data set. As in the case with M_2, M_3 captures the two qualitative features of the system (Supplementary Figures 9 and 10, red curve). It is notable that the computed residual is larger than $G(M_2)$, however, this is most likely the result of standard estimation error (e.g. non-optimal initial condition or insufficient search space). Alternatively, M_3 may represent a point at which the saturation of model benefit gained by increasing model complexity is saturated.

1.2.5 Summary

We generated and evaluated four candidate models, M_0, M_1, M_2, and M_3, with respect to how well each model captures the experimental observation, both quantitatively and qualitatively. M_0 did not capture the inflection observed in time-course degradation curves; M_1 did capture the inflection, but did not capture the nonlinear dose-response behavior; M_2 captures both the time-course and dose-response data qualitatively; and M_3 matches these behaviors with comparable quantitative metric to M_2. However, given the limitations of the experimental dataset (time-course to auxin step-input and auxin dose response), M_3, nor any more complex models, may not provide verifiable insights to the system. Said differently, more complex models may result in lower quantitative fit metric, however, to balance the estimation uncertainty associated with higher complexity models, we require richer perturbation of the system that reveals the appropriately higher complexity of the internal mechanism. Therefore, M_2 is arguably the simplest explanation for the observed phenomenon.

1.3 Parameter Reduction

Aside from M_0, the model candidates considered in the previous section include one or more internal states, x (and z), that are not readily associated with biological complexes. One way to approach this is to consider the internal state simply as a mathematical necessity for fitting the experimental observation. Another approach is to consider hypotheses as to what biological complex – that we know to exist in the auxin-mediated IAA degradation pathway – can be associated with x, and examine whether these hypotheses lend a useful quality to our model. One of the hypothetical interpretations of x is that it is a complex formed between auxin and AFB. A simple description of the mechanism in which IAA degrades in the presence of auxin and AFB is shown in Figure 1A, where auxin serves as a molecular glue, binding with an AFB and allowing the protein to bind with IAA, further triggering the ubiquitylation of IAA. Therefore, we postulate that x is a proxy of such a species.

Building on the hypothesis of model interpretation that x is a proxy of the auxin-bound AFB complex, we associate each of the model parameters to the identity of the two different proteins, IAA and AFB. Firstly, parameters k_1 and k_2 are rates associated with synthesis and degradation of auxin-bound receptor protein, where the synthesis is directly proportional to the input. In which case, we further hypothesized that these two parameters are dependent on the identity of AFB but are independent of the identity of the co-expressed IAA. Secondly, analogous interpretations are given to k_3 and k_4; these are rates of synthesis and basal (input-independent) degradation of IAA-YFP, and they are only dependent on the identity of the IAA and not on the identity of the AFB. Finally, k_5 is unique among the model parameters such that it is dependent on the identities of both proteins. Mathematically, k_5 is the rate constant for how fast the output degrades, and such a degradation process is proportional to the amount of x and y in

the system. One can then assign a biochemically feasible interpretation to the term, "when active AFB and IAA interact, the IAA degrades at a rate proportional to k_5". As shown in Figure 1C, the unifying feature of all IAA|AFB pairs is that they degrade when auxin is added to the system in varying degrees. Such variation in degradation among the IAA|AFB pairs can serve as a unique identifier for each pair, and we investigated whether a subset of parameters can serve as the quantitative identifier. Note that these association of parameters to reaction rates are based on a possible interpretation of the model, and should not be taken as a direct representation of a "true system". The parameters may be crude amalgamations of multiple biochemical processes but the resulting model is an elegant abstraction rid of unwieldy details.

In the previous section, when we fit candidate models to experimental data, all five of the M_2 parameters,

$$\theta_{ij}^{(2)} = \{k_1^{(i,j)}, k_2^{(i,j)}, k_3^{(i,j)}, k_4^{(i,j)}, k_5^{(i,j)}\}, \tag{11}$$

were allowed to vary, resulting in five different parameter values for each IAA|AFB pair[2]. This method, which allowed us to easily compare candidate models, makes it difficult to compare the parameters of one IAA|AFB pair to another. For example, suppose we want to directly compare the degradation rates of IAA17|TIR1 and IAA17|AFB2, which have mean fitted k_5 values of 0.034 and 0.21, respectively. The large discrepancy in the two values suggests a large difference in the respective degradation dynamics, but because each pair has other parameters that vary as well, the differences in k_5 are not the only explanation for the variation.

Therefore, we asked if some parameters may be common to a subset of the IAA|AFB pairs, and if consolidating these common parameters would reduce estimation uncertainty. This approach is often called global curve fitting. A systematic generation of all possible global fitting hypotheses for parameter reduction (identifying all possible combinations of common parameters across the 48 IAA|AFB pair, and five parameter model) would have been computationally expensive. Fortunately, the model interpretation provides a feasible guide as to which hypotheses are more likely than others, such as dividing the 48 pairs into smaller subsets. With this estimation approach, we can reduce the variability caused by other parameters and fairly compare parameter values. As mentioned before, k_5 is unique to the identity of each IAA|AFB pair, therefore, the parameter is the primary quantity of interest in comparing the differential degradation among the pairs.

First of all, we address an extreme case of parameter reduction, where we only let k_5 vary for all IAA|AFB pairs, and fix the rest of the parameters to be the same across all pairs. We denote this hypothesis H_1, which provides an additional constraint on the optimization problem, defined by

$$\begin{aligned} \min J(\theta^{(s)}, M_s) \quad &= \quad \sum_{i,j} \sum_{t_m \in \mathrm{T}} \left\| y_{ij}(t_m) - \hat{y}_{ij}(t_m, \theta_{ij}^{(s)}, M_s) \right\|_2, \\ \text{subject to} \qquad & k_l^{(i,j)} = k_l^{(i',j')} \qquad \forall i, i' \in \mathcal{I},\ \forall j, j' \in \mathcal{J},\ \text{and } l = 1,2,3,4, \end{aligned} \tag{12}$$

where, $\mathcal{I}$ and $\mathcal{J}$ denote the sets of IAA and AFB indices, respectively, and l denotes the parameter index. The resulting parameter vector, θ_{H_1}, has 52 distinct parameters (4 + 48 per pair) and results in $G(M_2, \theta_{H_1}) = 48.9$. Thus, H_1 reduces the cardinality of the parameter vector to the point where an IAA|AFB pair has only one parameter that differs from another pair. However, because H_1 makes both k_3 and k_4 be the same for all IAA|AFB pairs, it implies that the initial output value at $t = 0$ for all IAA|AFB pairs are equal ($y_{ij}(0) = k_3^{(i,j)}/k_4^{(i,j)}$). This is inconsistent with the experimental data where initial levels of expression vary (Figure S4). Therefore, H_1 is invalidated based on its conflict between the interpretation of the model and the experimental data.

[2] $k_l^{(i,j)}$ denotes the k_l value for $\mathrm{IAA}_i|\mathrm{AFB}_j$, where $l = 1,2,3,4,5$.

Next, we propose an alternative hypothesis to H_1 in which k_1, k_2, k_3 and k_4 are constrained, but across a smaller subset of IAA|AFB pairs. For example, it was shown that the AFBs do not have differential effect on basal dynamics of IAA (Supplementary Figure S4). Therefore, two IAA|AFB pairs with the same IAA have a similar initial output - suggesting equal k_3 and k_4 values for these two pairs. For this hypothesis, H_{11}, we have the following optimization constraints.

$$\text{subject to} \qquad k_l^{(i,j)} = k_l^{(i,j')} \qquad \forall j, j' \in \mathcal{J}, \text{ and } l = 1, 2, 3, 4. \tag{13}$$

The resulting parameter vector, denoted $\theta_{H_{11}}$, has 144 distinct parameters, and results in $G(M_2, \theta_{H_{11}}) = 24.33$. This decreased residual is a validation in which we let the model interpretation and the fundamental details of the system guide our hypotheses generation. To verify this approach, we generated an alternative hypothesis, H_{12}, where IAA|AFB pairs with the same AFB, versus those with the same IAA (H_{11}), have equal k_1, k_2, k_3 and k_4. This hypothesis has the same cost function as Eq 13 but with the following optimization constraint,

$$\text{subject to} \qquad k_l^{(i,j)} = k_l^{(i',j)} \qquad \forall i, i' \in \mathcal{I}, \text{ and } l = 1, 2, 3, 4. \tag{14}$$

Note that H_{12} was not generated based on the model interpretation as H_{11}, but was proposed as a counter example to our approach. The resulting residual is $G(M_2, \theta_{H_{12}}) = 36.62$, where $\theta_{H_{12}}$ has 56 distinct parameters. The increased residual validates our approach. Comparing H_1, H_{11} and H_{12} suggests that 1) larger numbers of distinct parameters tend to decrease the residual, and 2) when constraining the parameters across a smaller subset of IAA|AFB pairs, the model interpretation serves as a helpful guide in generating reasonable hypotheses.

The higher residuals of H_1 hypotheses family also suggest that for any two IAA|AFB pairs, more than one parameter ought to be allowed to vary (increasing degrees-of-freedom in the parameter estimation) to fit both data sets. Therefore, we further investigate whether a specific grouping of experimental data and parameter reduction hypotheses is possible. Each case of varying parameter (in addition to k_5), k_1, k_2, k_3 or k_4, is denoted with H_{21}, H_{22}, H_{23} or H_{24}, respectively (the four hypotheses are elements of the set $H_{2\kappa}$, where $\kappa = 1, 2, 3,$ or 4). Each hypothesis, depending on the parameter allowed to vary, is associated with data grouping that are supported by the model interpretation.

1. For H_{21} and H_{22}, the additional parameter allowed to vary is dependent on the identity of AFB and independent of the identity of the IAA. Therefore, IAA|AFB pairs are grouped by their IAAs (each group containing two pairs, IAA_i|TIR1 and IAA_i|AFB2), resulting in 24 distinct groups. For each group, the parameters are estimated under the constraint,

$$\text{subject to} \qquad k_l^{(i,j)} = k_l^{(i,j')} \qquad \forall j, j' \in \mathcal{J},\ l \in \{1, 2, 3, 4\} \backslash \{\kappa\}, \text{ and } \kappa = 1, 2. \tag{15}$$

   These hypotheses imply that a group of IAA|AFB pairs that have the same IAA have the same basal synthesis and degradation rates (k_3 and k_4) of the output. Furthermore, they imply that the variations among each group can be captured by varying k_5 and k_1 for H_{21}, or k_5 and k_2 for H_{22}.

2. For H_{23} and H_{24}, the additional parameter allowed to vary is dependent on the identity of IAA and independent of the identity of the AFB. Therefore, IAA|AFB pairs are grouped by their AFBs (each group containing 24 pairs, IAA_i|AFB, where $i = [1, \cdots, 24]$), resulting in two groups. For each group, the parameters are estimated under the constraint,

$$\text{subject to} \qquad k_l^{(i,j)} = k_l^{(i',j)} \qquad \forall i, i' \in \mathcal{I},\ l \in \{1, 2, 3, 4\} \backslash \{\kappa\}, \text{ and } \kappa = 3, 4. \tag{16}$$

   The hypotheses imply that a group of IAA|AFB pairs that have the same AFB has the same synthesis and degradation rates of the internal state (k_1 and k_2). Furthermore, they imply that the variations among each group can be captured by varying k_5 and k_3 for H_{23}, or k_5 and k_4 for H_{24}.

Supplementary Table 3 shows the residuals and the number of distinct parameters for various hypotheses investigated. Compared to H_1 hypotheses, H_2 hypotheses tend to have lower residuals, owing to the larger degrees-of-freedom given in the estimation constraints. Additionally, H_{24} has the lowest residual even with the lowest number of distinct parameters. This suggests that for any two IAA|AFB pairs, the differential dynamics between the two can be captured through varying the basal rate parameters of IAA and the input-mediated degradation by the AFBs (k_5). These two dynamics, however, are independent of one another as discussed previously (Results, Figure 2). Also, single parameter variation studies suggests that a set of time-courses predicted by varying k_3 or k_4 have identical degradation profiles when normalized to their initial conditions (Supplementary Figure 11, Supplementary Table 7). The simulation study is also supported by experimental data of IAA1 and IAA1.1, where IAA1.1 is a codon-optimized version of IAA1. This results in higher expression level for IAA1.1 relative to IAA1, which under the model interpretation, is equivalent to increasing k_3 and leaving other parameters the same. When the two curves are normalized to their initial conditions (Supplementary Figure 9), the curves overlap closely. This is reflected by the close k_5 values of IAA1 and IAA1.1 (Supplementary Table 4 and 5).

The normalized degradation curves in Supplementary Figure 11 further provide two notable features of the model. First, they suggest that the two parameter k_3 and k_4 are, in fact, dependent parameters that can be consolidated into a single parameter by normalizing the output. The normalized version of M_2 is

$$\frac{dx(t)}{dt} = k_1\, u(t) - k_2\, x(t) \tag{17}$$

$$\frac{dz(t)}{dt} = k_4 - k_4\, z(t) - k_5\, x(t)\, z(t), \tag{18}$$

where $z = \frac{y}{y_0} = \frac{k_4}{k_3}\, y$, the output normalized to its initial value. This procedure further reduces the number of parameters to be estimated and decreases computational cost in estimation. The differences in the estimated values of k_5 are negligible between the two versions of model. A second notable feature of the model is that the range of degradation profiles in experimental data can be fitted just as well by varying k_1 instead of k_5. This feature is not surprising as varying k_1 increase the rate at which x increases, ultimately having the same effect on the output. However, because of the way we interpret the model parameters, k_1 is independent of the identity of IAA. This conflicts with our objective of identifying a degradation rate parameter that are unique to each IAA|AFB pair. Therefore, we choose k_5 as the single parameter that captures the differential degradation range we observe among the IAA|AFB pairs.

1.4 Summary

Through iterative searches in model discrimination and parameter reduction, we identified a single parameter that captures the differential degradation exhibited by the family of IAA|AFB pairs. The reasoning behind finding a single parameter is largely inspired by the engineering principles of modularity and composable parts. For example, an electric circuit is composed of individual modular parts, such as resistors and transistors. The function of the circuit is tunable by swapping out these modular parts, where the electrical functionality of each type of modular part is specified by a number (i.e. a resistor is specified by its resistance). Casting this principle on the auxin signaling pathway, we ask whether the IAA|AFB pair degradation module (in the larger scheme of the auxin signal pathway) is a modular part, and if so, whether the biological functionality of the module can be specified by a number. The functional feature of the IAA|AFB module, degradation, demonstrates a large range of responses. Therefore, we hypothesize that the number that specifies each IAA|AFB pair's unique biological functionality is its degradation rate (k_5).

Now that we have a data-sheet of k_5 for a large group of IAA|AFB pair, the hypothesis regarding the modularity of these pairs must be verified. It will require an auxin synthetic network containing an IAA|AFB pair, where the part can be easily replaced with another pair. Using a similar approach, a succinct mathematical representation of such a network can be devised, and preferably, the k_5 identified

in this work will be a part of such a model. If a coherent function that maps the differential degradation rates (caused by using different IAA|AFB pairs) and the differential outputs of the larger network can be identified, it will allow us to test to what extent and under what context these pairs are modular. And if this is not the case, the question remains whether there is another set of identifiable quantities for the IAA|AFB pairs that is a better specification of their biological functionality and predictors of the composite network output. Furthermore, the relationship between the k_5 and the output of the network will illuminate the core interactions within the network, aiding in increasingly accurate mathematical representations of the synthetic network. These approaches will not only answer questions regarding the engineerability of auxin signaling pathway, but also provide the basis for novel ways of system identification in biology.

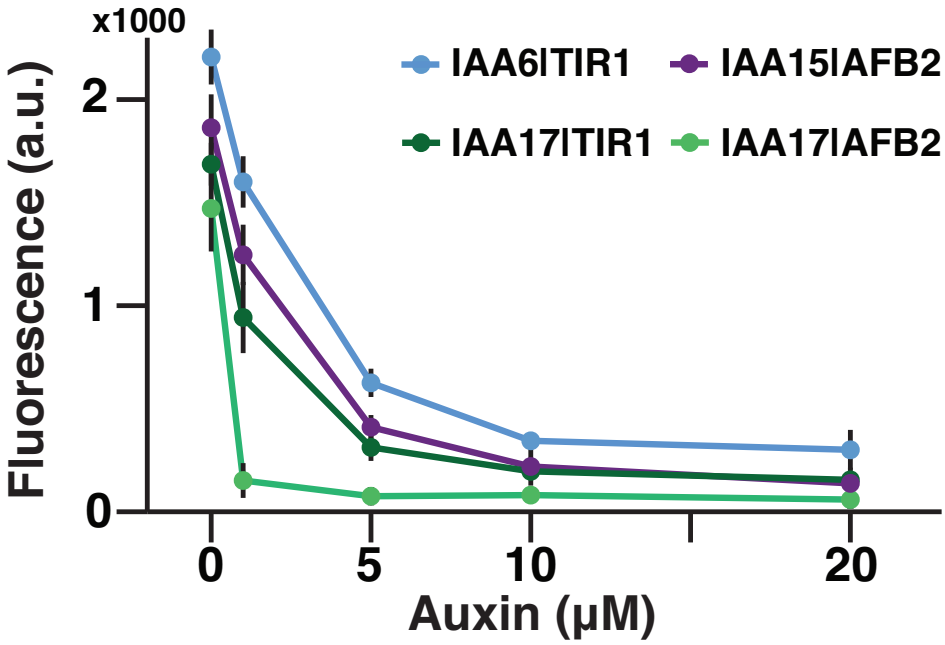

Supplementary Figure 1: Addition of 10μM auxin is sufficient for maximal degradation of IAAs. IAAs with the slowest and fastest degradation rates for TIR1 (IAA6 and IAA17, respectively) and AFB2 (IAA15 and IAA17, respectively) were treated with increasing concentrations of auxin. Fluorescence levels were measured two hours after auxin treatment. Doses of 10μM and 20μM resulted similar levels of degradation. Error bars represent $\pm$ one standard deviation between two experiments performed on different days.

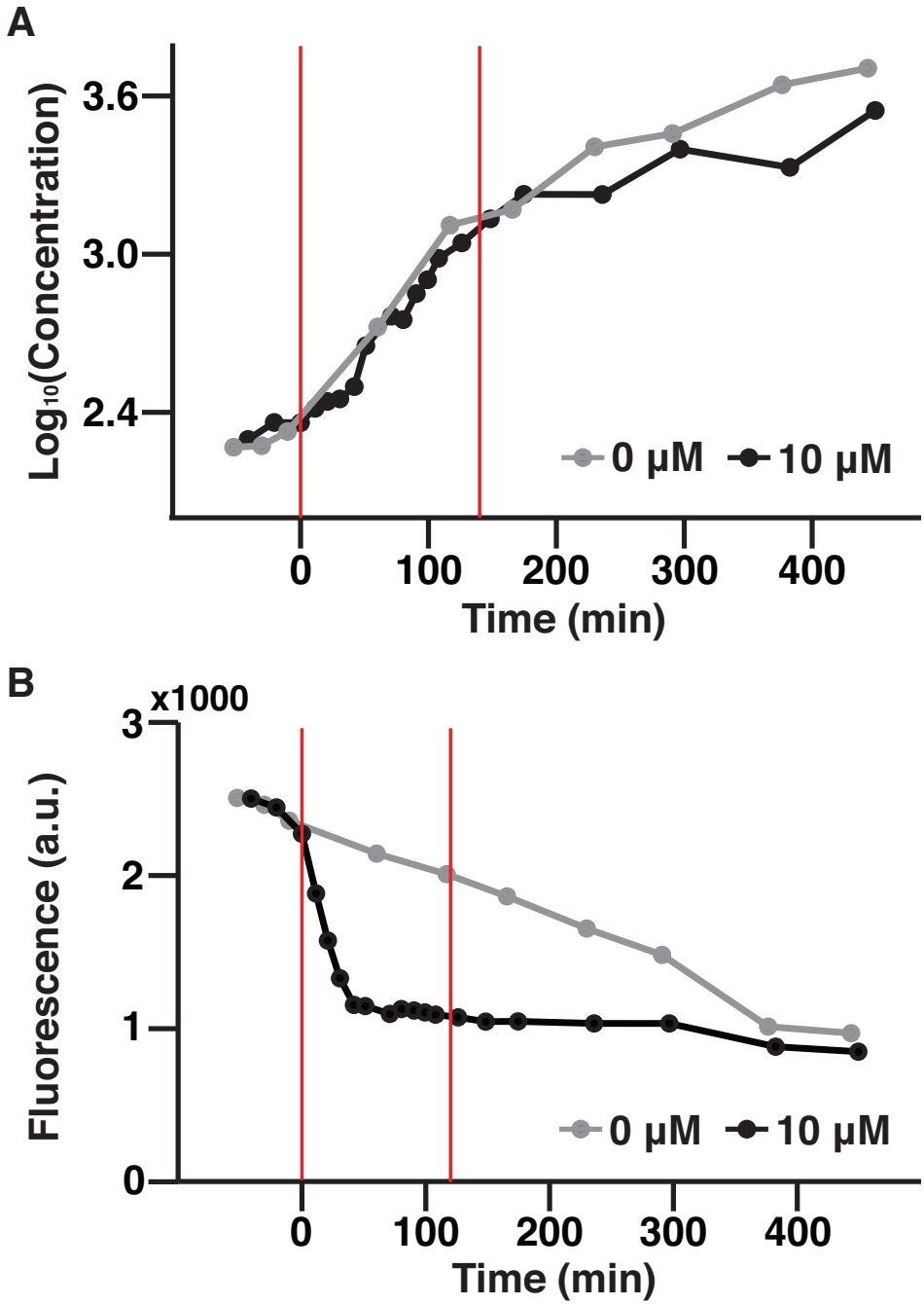

Supplementary Figure 2: Fluorescence levels decrease drastically as yeast cells enter stationary phase. (A) Representative graphs of yeast growth over time of cells containing IAA1|TIR1 treated with mock (grey) or with 10μM auxin (black). (B) Fluorescence in the same cells over time. Red lines demarcate window of experimental data collection.

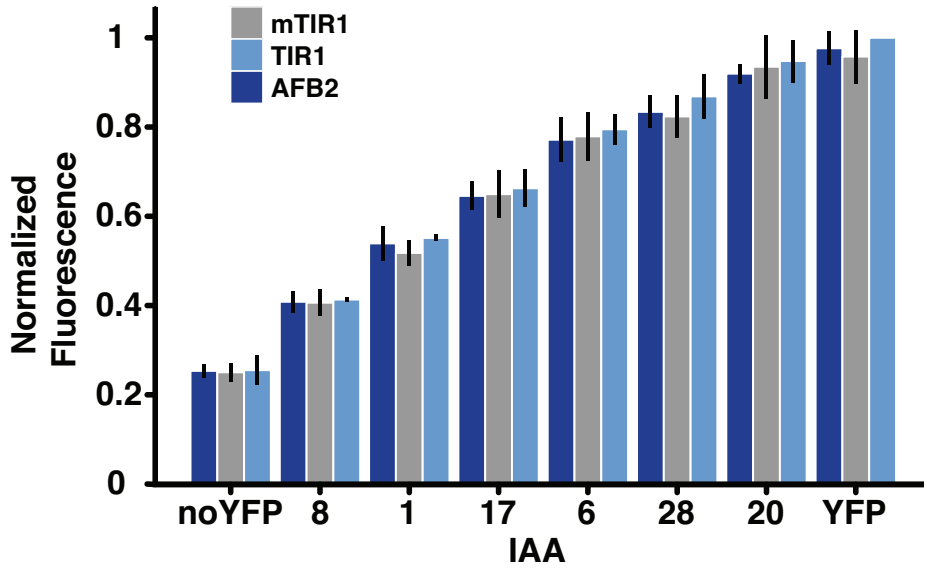

Supplementary Figure 3: AFBs do not have differential effects on basal degradation of IAAs. A sample set of IAAs was co-expressed with mTIR1, TIR1, or AFB2. Fluorescence at steady state, prior to auxin addition, was measured. These IAAs were chosen as they span the range of observed initial steady state intensity values. The noYFP strain expresses an allele of IAA17 without a YFP fusion. Regardless of AFB identity, initial fluorescence levels were indistinguishable for a given IAA. Strains were prepared as in Figure 1C. Each experiment was normalized to the YFP—TIR1 expression level. Error bars are ± one standard deviation between three experiments performed on different days.

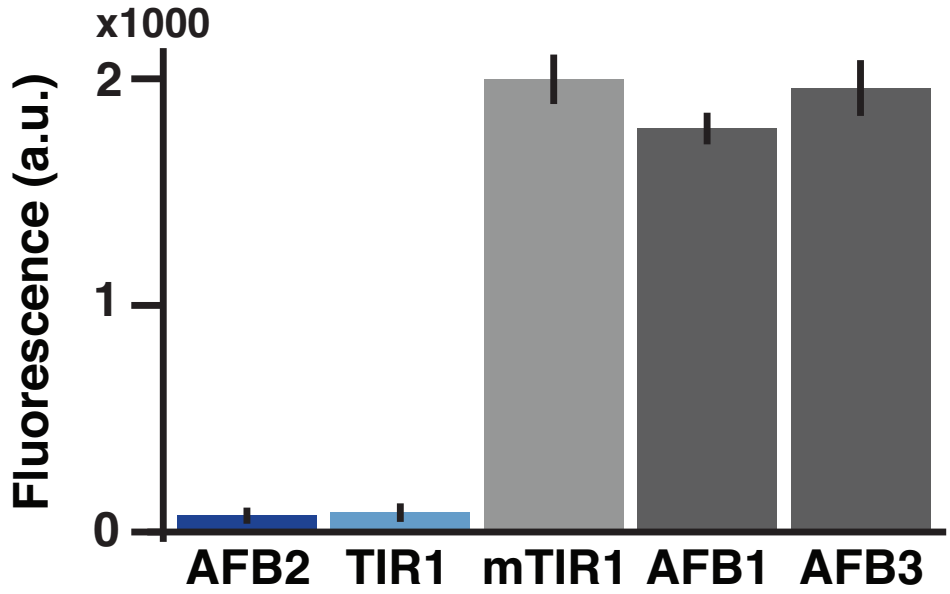

Supplementary Figure 4: AFB1 and AFB3 do not promote degradation of IAA2. IAA2 was co-expressed with each of five receptor types. Fluorescence levels were measured after a 3-hour treatment with 20μM auxin. Similar to mTIR1, AFB1 and AFB3 failed to exhibit degradation of IAA2. Error bars represent $\pm$ one standard deviation between two replicates.

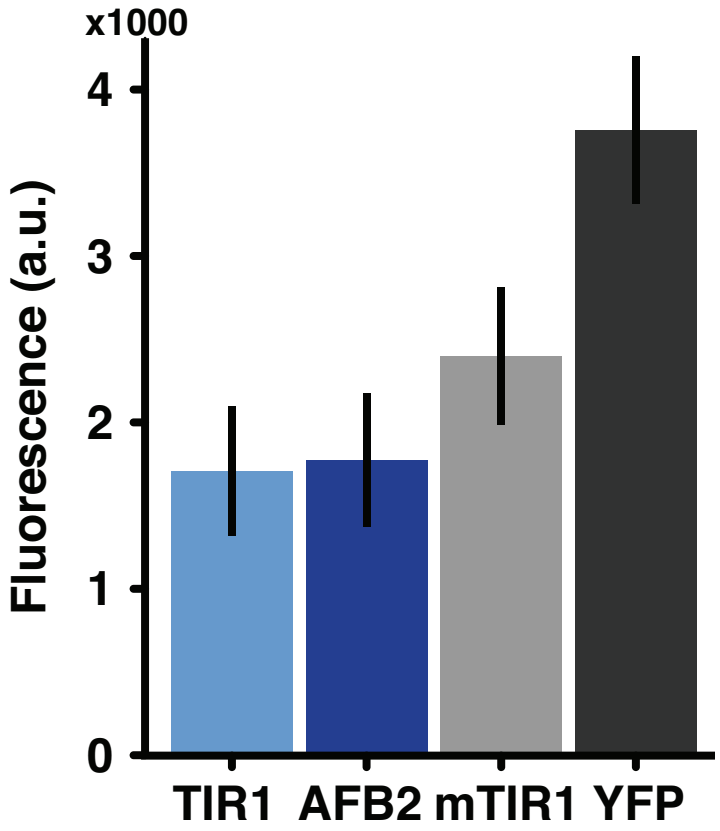

Supplementary Figure 5: TIR1 is expressed at a similar level to AFB2. AFB-YFP constructs were singly integrated into yeast, and their fluorescence intensities were compared using flow-cytometry. Error bars represent one standard deviation, between three replicates.

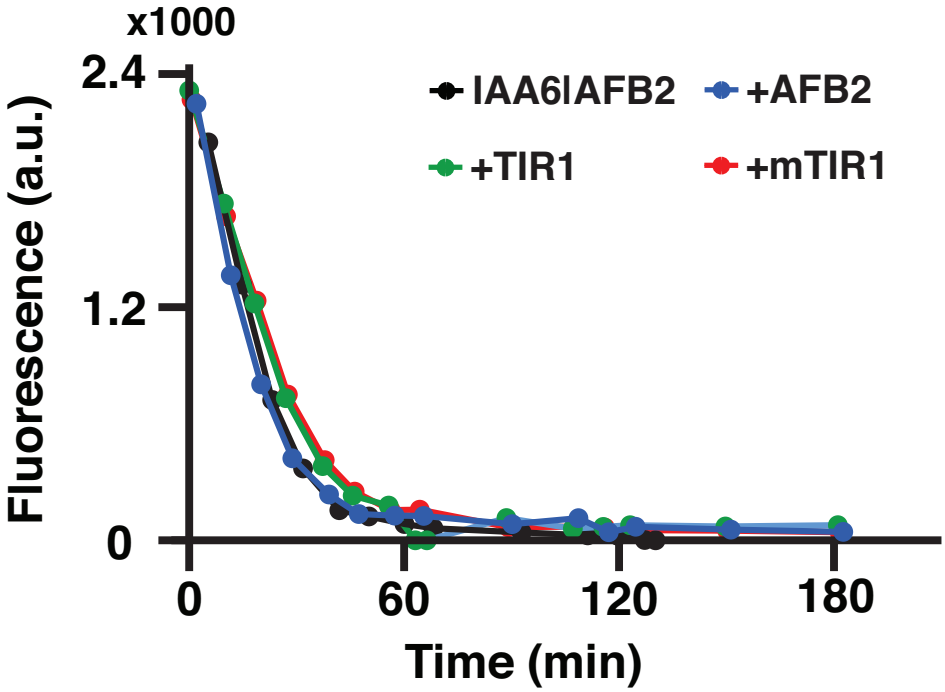

Supplementary Figure 6: AFB2 expression is not rate limiting. Additional copies of AFB (blue), TIR1 (green) or mTIR1 (red) were co-expressed with IAA6|AFB2 in diploid cells. These were compared to the original IAA6|AFB2 strain (black line). The overlapping curves indicate that the degradation rates are similar, implying that with IAA6, the effect of AFB2 is dominant relative to TIR1, and its activity is not increased with additional copies of the gene.

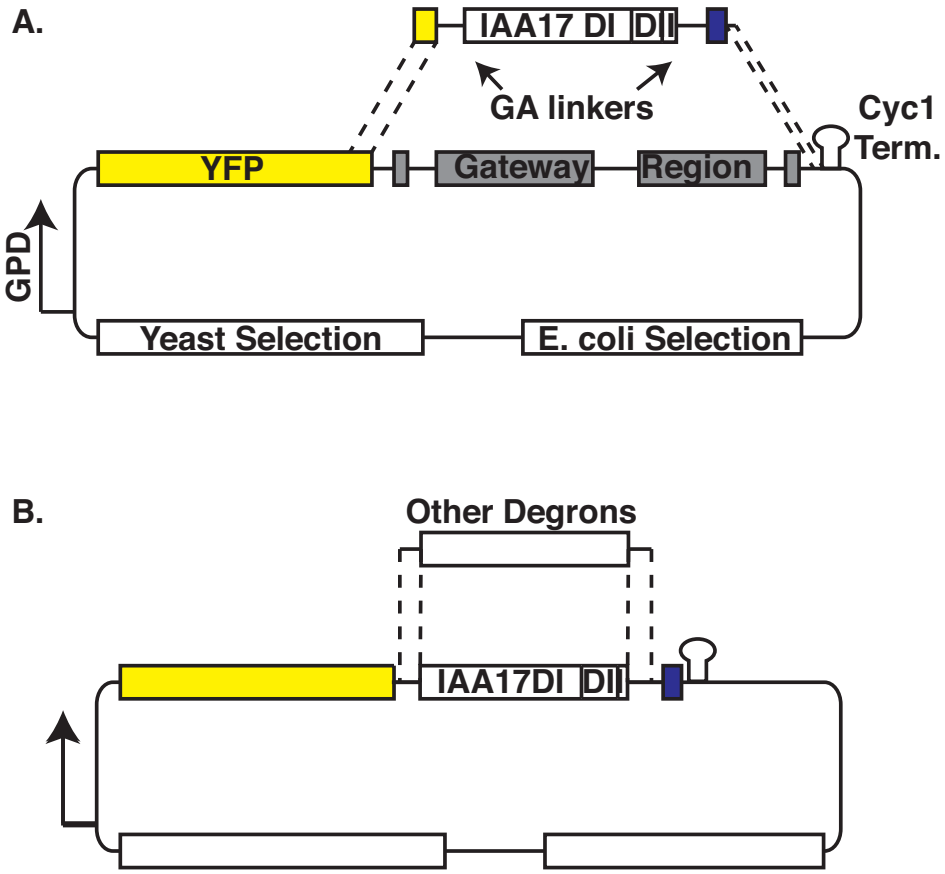

Supplementary Figure 7: Schematic of cloning strategy for domain II truncations. (A) IAA17.T1 was synthesized with Gly-Ala linkers and a 2XSV40-NLS at the C-terminus. This fragment was amplified with primers listed in Table S9 and cloned using Gibson assembly [3]. (B) Gibson assembly was then used to insert other IAA truncations into the same NLS-containing plasmid backbone.

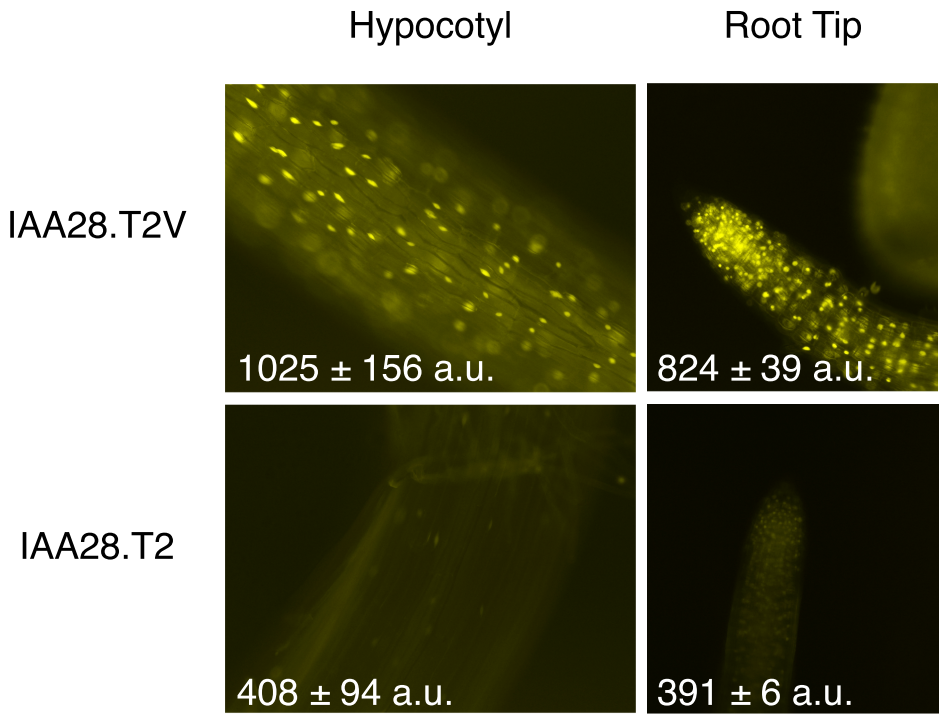

Supplementary Figure 8: Yeast degradation experiments predict relative degradation rates in plants. Consistent with the truncation degradation rates observed in yeast (Fig. 3B), hypocotyls and root tips of plants expressing IAA28.T2-VENUS accumulated lower fluorescence levels than those expressing DII-VENUS (identical to IAA28.T2V) [2]. Mean fluorescence intensity ± SEM values are shown with representative images.

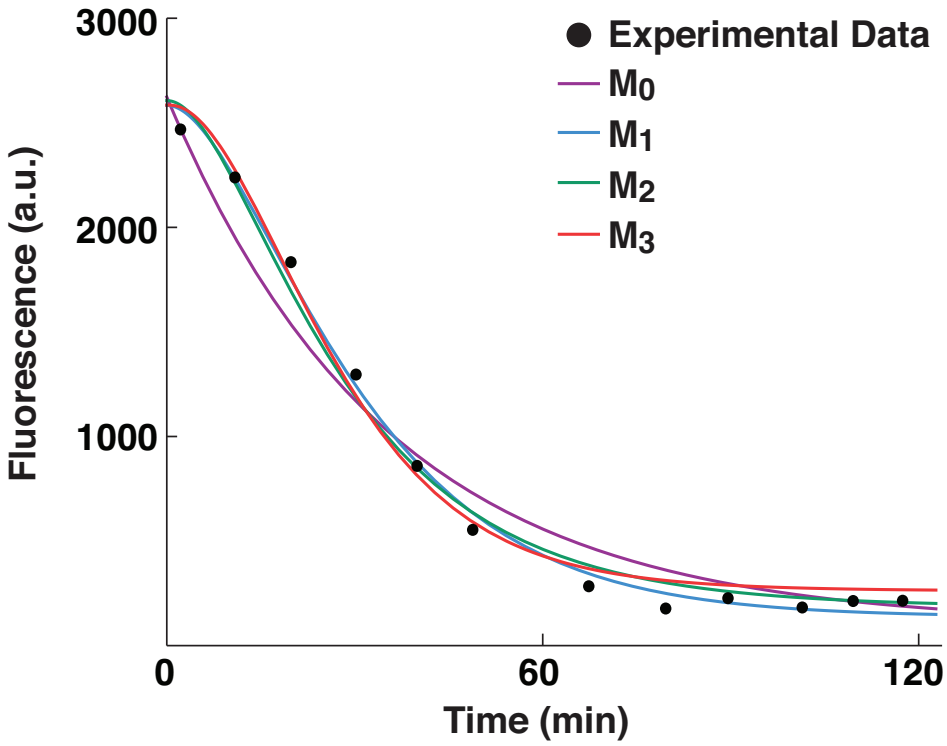

Supplementary Figure 9: Sample time-course IAA degradation data and model fits of IAA14|TIR1. Experimental data are shown in black circles, and the fits are shown in purple, blue, green and red for M_0, M_1, M_2 and M_3 models, respectively.

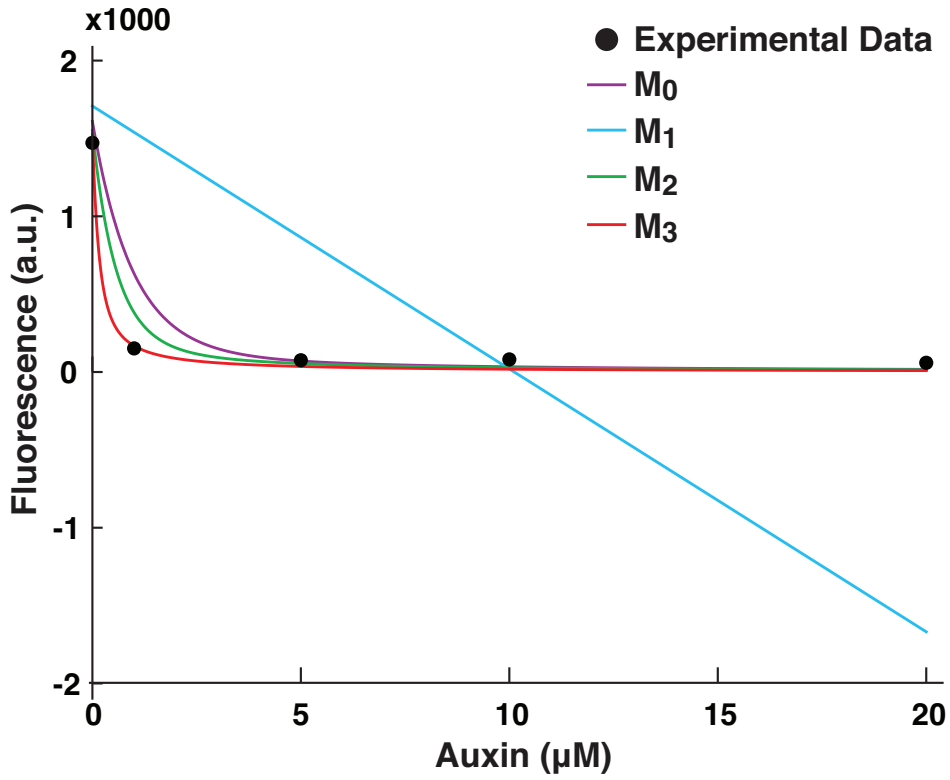

Supplementary Figure 10: Sample dose-response data and model predicted dose-response of IAA17|AFB2. Experimental data are shown in black circles, and the fits are shown in purple, blue, green and red for M_0, M_1, M_2, and M_3 models, respectively.

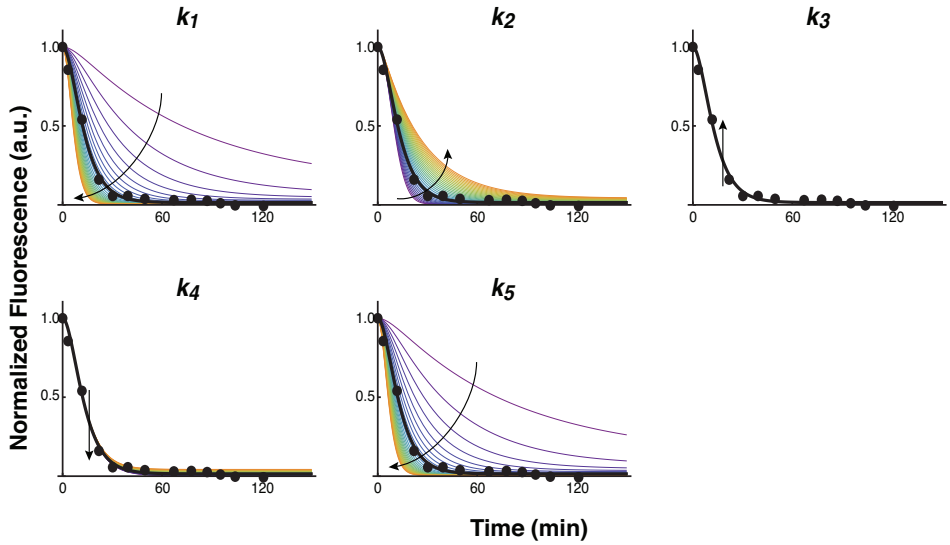

Supplementary Figure 11: Parameter variations study of M_2. Parameters of M_2 are varied from 10% to 300% of the nominal (estimated) values for IAA17|AFB2. The range was chosen based on the demonstrated range of estimated parameters shown in Supplementary Table 7. The trend demonstrated here is general for all IAA |AFB pairs. The resulting degradation curves are normalized to its initial condition. The experimental data are shown in black dots and the black arrows indicate the direction of parameter value increase.

Supplementary Table 1. A table of degradation rates, half-lives, and affinities from yeast, *in vitro* and plant studies.

AFB	IAA	Havens, 2012[1]		Calderon, 2012[2]	Dreher , 2006[3*]		Ramos, 2001[4*]	Quellet, 2001[5*]	Gray, 2001[6*]
		k5 mean	t 1/2 mean	Kd	basal half-life	auxin half-life	basal half-life	basal half-life	basal half-life
TIR1	1	3.94E-02	24.6	44.33	11.8	-	8	-	-
TIR1	1.1	3.49E-02	26.6	-	-	-	-	-	-
TIR1	2	3.84E-02	25.0	-	-	-	-	-	-
TIR1	3	2.90E-02	30.1	16.97	-	-	-	-	-
TIR1	4	2.59E-02	32.6	-	-	-	-	-	-
TIR1	6	2.01E-02	38.8	-	-	-	-	-	-
TIR1	7	3.52E-02	26.5	17	-	-	-	-	10.8
TIR1	8	4.10E-02	24.3	-	-	-	-	-	-
TIR1	9	3.70E-02	25.6	-	19	-	-	-	-
TIR1	10	2.65E-02	32.1	-	-	-	-	-	-
TIR1	11	1.24E-02	54.7	-	-	-	-	-	-
TIR1	12	3.06E-02	29.2	270	-	-	-	-	-
TIR1	13	3.81E-02	25.1	-	-	-	-	-	-
TIR1	14	3.11E-02	28.8	10.1	-	-	-	-	-
TIR1	15	2.02E-02	38.6	-	-	-	-	-	-
TIR1	17	3.63E-02	26.1	33	10.0	4.8	-	80.0	-
TIR1	18	3.20E-02	28.2	-	-	-	-	-	-
TIR1	19	2.82E-02	30.9	-	-	-	-	-	-
TIR1	20	2.88E-03	>>>	-	>>>	>>>	-	-	-
TIR1	26	2.75E-02	31.3	-	-	-	-	-	-
TIR1	27	3.48E-02	26.7	-	-	-	-	-	-
TIR1	28	2.55E-02	33.1	75	79.3	14.8	-	-	-
TIR1	31	5.55E-03	89.1	>1000	>20 hr	4 hr	-	-	-
TIR1	32	4.60E-03	>>>	-	-	-	-	-	

AFB	IAA	Havens, 2012[1]		Calderon, 2012[2]	Dreher , 2006[3*]		Ramos, 2001[4*]	Quellet, 2001[5*]	Gray, 2001[6*]
		k5 mean	t 1/2 mean	Kd	basal half-life	auxin half-life	basal half-life	basal half-life	basal half-life
AFB2	1	4.52E-02	19.3	-	-	-	-	-	-
AFB2	1.1	4.03E-02	20.9	-	-	-	-	-	-
AFB2	2	4.24E-02	20.3	-	-	-	-	-	-
AFB2	3	5.71E-02	16.8	-	-	-	-	-	-
AFB2	4	5.96E-02	16.3	-	-	-	-	-	-
AFB2	6	6.57E-02	15.4	-	-	-	-	-	-
AFB2	7	8.07E-02	13.6	-	-	-	-	-	-
AFB2	8	9.78E-02	12.2	-	-	-	-	-	-
AFB2	9	6.44E-02	15.7	-	-	-	-	-	-
AFB2	10	5.19E-02	17.7	-	-	-	-	-	-
AFB2	11	2.06E-02	31.8	-	-	-	-	-	-
AFB2	12	5.00E-02	18.1	-	-	-	-	-	-
AFB2	13	5.00E-02	18.3	-	-	-	-	-	-
AFB2	14	6.87E-02	15.0	-	-	-	-	-	-
AFB2	15	2.38E-02	29.0	-	-	-	-	-	-
AFB2	17	1.08E-01	11.5	-	-	-	-	-	-
AFB2	18	5.25E-02	17.7	-	-	-	-	-	-
AFB2	19	6.50E-02	15.6	-	-	-	-	-	-
AFB2	20	2.85E-03	>>>	-	-	-	-	-	-
AFB2	26	4.09E-02	20.7	-	-	-	-	-	-
AFB2	27	6.18E-02	15.9	-	-	-	-	-	-
AFB2	28	4.13E-02	20.5	-	-	-	-	-	-
AFB2	31	1.06E-02	48.9	-	-	-	-	-	-
AFB2	32	3.38E-03	>>>	-	-	-	-	-	-

[1] YFP-IAA|AFB pairs were co-expressed in yeast and YFP levels were monitored after the addition of 10 mM IAA. k5 and t 1/2 were calculated using data-driven model (Fig. 2)

[2] In vitro radio-labeled auxin binding assays were performed using purified ASK1-TIR1 complexes expressed in insect cells and GST-tagged IAAs expressed in *E.coli.*

[3] IAA:LUC transgenic seedlings were treated with cyclohexamide and LUC levels assayed at multiple time intervals. For auxin half-lives , seedlings were pretreated with 2,4-D for two hours prior to the addition of cyclohexamide The data was normalized to the mock treated samples and linearized by taking the natural log. The eqn of the linear best fit line was used to calc half-lives.

[4] IAA:LUC transgenic seedlings were treated with cyclohexamide and LUC levels assayed at multiple time intervals.

[5] Pulse-chase experiments were utlized to calculate the half-life of endogenous IAA17 in WT dark grown seedlings.

[6] Pulse-chase experiments were utlized to calculate the half-life of endogenous IAA7 in WT seedlings using the formula $t1/2 = 0.693t/\ln(N0/Nx)$, where t is time in minutes and N0 and Nx equal the amounts of AXR2 at t = 0 and t = 30min.

* Assays performed in whole seedlings: cannot distinguish receptor(s) responsible for degradation. Values are listed in the TIR1 category as TIR1 is presumed to be the dominant receptor *in planta,* though multiple receptors may play a role.

Supplementary Table 2: Table of amino acids included in each IAA truncation. The position of the conserved 13 amino acid domain II is included for comparison.

Truncation	Domains	Amino Acids		
		IAA1	IAA6	IAA28
Full Length (FL)	DI-DIV	1-168	1-189	1-175
T1	D1 and DII	1-75	1-94	1-81
T2	DII + additional aa	41-75	62-94	43-81
T2V	DII + additional aa	NA	NA	28-61
Conserved Core	DII alone	55-67	70-82	48-60

Supplementary Table 3: The residuals and the number of distinct parameters for M_0, M_1, M_2 (including its hypotheses), and M_3.

Hypothesis	$G(M)$	Number of distinct parameters for 48 IAA|Fbox pairs
H_0	49.31	144
H_1	81.68	240
H_2	24.54	240
H_{21}	32.29	168
H_{22}	46.32	168
H_{23}	48.11	102
H_{24}	27.44	102
H_3	30.63	336

Supplementary Table 4: Estimated parameters for IAA|TIR1 pairs using H_{23}.

Fbox	IAA	Replicate	k_1	k_2	k_3	k_4	k_5
TIR1	1	1	1.08E-01	9.22E-02	4.29E+00	3.14E-03	3.44E-02
TIR1	1.1	1	1.08E-01	9.22E-02	8.69E+00	3.14E-03	3.22E-02
TIR1	2	1	1.08E-01	9.22E-02	6.86E+00	3.14E-03	3.54E-02
TIR1	3	1	1.08E-01	9.22E-02	9.03E+00	3.14E-03	2.62E-02
TIR1	4	1	1.08E-01	9.22E-02	9.74E+00	3.14E-03	2.58E-02
TIR1	6	1	1.08E-01	9.22E-02	8.44E+00	3.14E-03	2.02E-02
TIR1	7	1	1.08E-01	9.22E-02	7.62E+00	3.14E-03	3.05E-02
TIR1	8	1	1.08E-01	9.22E-02	3.29E+00	3.14E-03	3.17E-02
TIR1	9	1	1.08E-01	9.22E-02	7.39E+00	3.14E-03	3.34E-02
TIR1	10	1	1.08E-01	9.22E-02	5.02E+00	3.14E-03	2.55E-02
TIR1	11	1	1.08E-01	9.22E-02	4.61E+00	3.14E-03	9.46E-03
TIR1	12	1	1.08E-01	9.22E-02	8.91E+00	3.14E-03	2.67E-02
TIR1	13	1	1.08E-01	9.22E-02	8.24E+00	3.14E-03	3.54E-02
TIR1	14	1	1.08E-01	9.22E-02	5.16E+00	3.14E-03	3.17E-02
TIR1	15	1	1.08E-01	9.22E-02	6.67E+00	3.14E-03	1.91E-02
TIR1	17	1	1.08E-01	9.22E-02	6.74E+00	3.14E-03	3.03E-02
TIR1	18	1	1.08E-01	9.22E-02	7.44E+00	3.14E-03	2.89E-02
TIR1	19	1	1.08E-01	9.22E-02	5.71E+00	3.14E-03	2.41E-02
TIR1	20	1	1.08E-01	9.22E-02	9.99E+00	3.14E-03	2.21E-03
TIR1	26	1	1.08E-01	9.22E-02	8.03E+00	3.14E-03	2.66E-02
TIR1	27	1	1.08E-01	9.22E-02	4.06E+00	3.14E-03	3.18E-02
TIR1	28	1	1.08E-01	9.22E-02	8.20E+00	3.14E-03	2.09E-02
TIR1	31	1	1.08E-01	9.22E-02	6.72E+00	3.14E-03	4.88E-03
TIR1	32	1	1.08E-01	9.22E-02	2.47E+00	3.14E-03	3.81E-03
TIR1	1	2	1.42E-01	1.72E-01	3.89E+00	3.19E-03	4.43E-02
TIR1	1.1	2	1.42E-01	1.72E-01	9.00E+00	3.19E-03	3.77E-02
TIR1	2	2	1.42E-01	1.72E-01	5.77E+00	3.19E-03	4.14E-02
TIR1	3	2	1.42E-01	1.72E-01	8.67E+00	3.19E-03	3.19E-02
TIR1	4	2	1.42E-01	1.72E-01	1.05E+01	3.19E-03	2.59E-02
TIR1	6	2	1.42E-01	1.72E-01	8.79E+00	3.19E-03	2.00E-02
TIR1	7	2	1.42E-01	1.72E-01	7.07E+00	3.19E-03	4.00E-02
TIR1	8	2	1.42E-01	1.72E-01	2.92E+00	3.19E-03	5.02E-02
TIR1	9	2	1.42E-01	1.72E-01	7.56E+00	3.19E-03	4.07E-02
TIR1	10	2	1.42E-01	1.72E-01	4.76E+00	3.19E-03	2.74E-02
TIR1	11	2	1.42E-01	1.72E-01	4.71E+00	3.19E-03	1.54E-02
TIR1	12	2	1.42E-01	1.72E-01	8.83E+00	3.19E-03	3.45E-02
TIR1	13	2	1.42E-01	1.72E-01	8.46E+00	3.19E-03	4.07E-02
TIR1	14	2	1.42E-01	1.72E-01	5.32E+00	3.19E-03	3.05E-02
TIR1	15	2	1.42E-01	1.72E-01	5.71E+00	3.19E-03	2.14E-02
TIR1	17	2	1.42E-01	1.72E-01	6.30E+00	3.19E-03	4.23E-02
TIR1	18	2	1.42E-01	1.72E-01	8.19E+00	3.19E-03	3.51E-02
TIR1	19	2	1.42E-01	1.72E-01	5.39E+00	3.19E-03	3.22E-02
TIR1	20	2	1.42E-01	1.72E-01	9.59E+00	3.19E-03	3.54E-03
TIR1	26	2	1.42E-01	1.72E-01	9.27E+00	3.19E-03	2.85E-02
TIR1	27	2	1.42E-01	1.72E-01	3.92E+00	3.19E-03	3.78E-02
TIR1	28	2	1.42E-01	1.72E-01	7.87E+00	3.19E-03	3.02E-02
TIR1	31	2	1.42E-01	1.72E-01	6.81E+00	3.19E-03	6.23E-03
TIR1	32	2	1.42E-01	1.72E-01	2.55E+00	3.19E-03	5.39E-03

Supplementary Table 5: Estimated parameters for IAA|AFB2 pairs using H_{23}.

Fbox	IAA	Replicate	k_1	k_2	k_3	k_4	k_5
AFB2	1	1	1.49E-01	1.18E-01	4.48E+00	3.63E-03	4.59E-02
AFB2	1.1	1	1.49E-01	1.18E-01	9.77E+00	3.63E-03	4.47E-02
AFB2	2	1	1.49E-01	1.18E-01	8.09E+00	3.63E-03	4.65E-02
AFB2	3	1	1.49E-01	1.18E-01	1.13E+01	3.63E-03	6.14E-02
AFB2	4	1	1.49E-01	1.18E-01	1.16E+01	3.63E-03	6.05E-02
AFB2	6	1	1.49E-01	1.18E-01	8.55E+00	3.63E-03	7.06E-02
AFB2	7	1	1.49E-01	1.18E-01	7.19E+00	3.63E-03	8.35E-02
AFB2	8	1	1.49E-01	1.18E-01	3.16E+00	3.63E-03	1.05E-01
AFB2	9	1	1.49E-01	1.18E-01	8.01E+00	3.63E-03	7.29E-02
AFB2	10	1	1.49E-01	1.18E-01	5.80E+00	3.63E-03	5.16E-02
AFB2	11	1	1.49E-01	1.18E-01	5.87E+00	3.63E-03	2.08E-02
AFB2	12	1	1.49E-01	1.18E-01	9.16E+00	3.63E-03	5.04E-02
AFB2	13	1	1.49E-01	1.18E-01	9.57E+00	3.63E-03	5.52E-02
AFB2	14	1	1.49E-01	1.18E-01	6.25E+00	3.63E-03	6.45E-02
AFB2	15	1	1.49E-01	1.18E-01	7.94E+00	3.63E-03	2.47E-02
AFB2	17	1	1.49E-01	1.18E-01	6.04E+00	3.63E-03	1.04E-01
AFB2	18	1	1.49E-01	1.18E-01	8.57E+00	3.63E-03	5.80E-02
AFB2	19	1	1.49E-01	1.18E-01	5.96E+00	3.63E-03	5.65E-02
AFB2	20	1	1.49E-01	1.18E-01	1.07E+01	3.63E-03	2.67E-03
AFB2	26	1	1.49E-01	1.18E-01	1.06E+01	3.63E-03	4.42E-02
AFB2	27	1	1.49E-01	1.18E-01	4.49E+00	3.63E-03	6.19E-02
AFB2	28	1	1.49E-01	1.18E-01	8.85E+00	3.63E-03	4.14E-02
AFB2	31	1	1.49E-01	1.18E-01	7.50E+00	3.63E-03	1.07E-02
AFB2	32	1	1.49E-01	1.18E-01	2.85E+00	3.63E-03	2.51E-03
AFB2	1	2	1.27E-01	8.77E-02	3.72E+00	3.25E-03	4.46E-02
AFB2	1.1	2	1.27E-01	8.77E-02	9.23E+00	3.25E-03	3.59E-02
AFB2	2	2	1.27E-01	8.77E-02	7.84E+00	3.25E-03	3.82E-02
AFB2	3	2	1.27E-01	8.77E-02	8.45E+00	3.25E-03	5.28E-02
AFB2	4	2	1.27E-01	8.77E-02	1.02E+01	3.25E-03	5.87E-02
AFB2	6	2	1.27E-01	8.77E-02	8.10E+00	3.25E-03	6.08E-02
AFB2	7	2	1.27E-01	8.77E-02	6.33E+00	3.25E-03	7.79E-02
AFB2	8	2	1.27E-01	8.77E-02	2.66E+00	3.25E-03	9.07E-02
AFB2	9	2	1.27E-01	8.77E-02	7.16E+00	3.25E-03	5.58E-02
AFB2	10	2	1.27E-01	8.77E-02	5.49E+00	3.25E-03	5.23E-02
AFB2	11	2	1.27E-01	8.77E-02	5.63E+00	3.25E-03	2.04E-02
AFB2	12	2	1.27E-01	8.77E-02	8.07E+00	3.25E-03	4.96E-02
AFB2	13	2	1.27E-01	8.77E-02	8.90E+00	3.25E-03	4.47E-02
AFB2	14	2	1.27E-01	8.77E-02	5.43E+00	3.25E-03	7.30E-02
AFB2	15	2	1.27E-01	8.77E-02	7.37E+00	3.25E-03	2.29E-02
AFB2	17	2	1.27E-01	8.77E-02	5.05E+00	3.25E-03	1.12E-01
AFB2	18	2	1.27E-01	8.77E-02	8.16E+00	3.25E-03	4.71E-02
AFB2	19	2	1.27E-01	8.77E-02	4.67E+00	3.25E-03	7.35E-02
AFB2	20	2	1.27E-01	8.77E-02	9.29E+00	3.25E-03	3.03E-03
AFB2	26	2	1.27E-01	8.77E-02	9.99E+00	3.25E-03	3.77E-02
AFB2	27	2	1.27E-01	8.77E-02	3.93E+00	3.25E-03	6.17E-02
AFB2	28	2	1.27E-01	8.77E-02	7.56E+00	3.25E-03	4.12E-02
AFB2	31	2	1.27E-01	8.77E-02	6.90E+00	3.25E-03	1.06E-02
AFB2	32	2	1.27E-01	8.77E-02	2.68E+00	3.25E-03	4.25E-03

Supplementary Table 6: Estimated parameters for Degron comparison study using H_{23}.

Fbox	IAA	Degron	Replicate	k_1	k_2	k_3	k_4	k_5
TIR1	1	FL	1	1.08E-01	9.22E-02	6.51E+00	3.14E-03	3.98E-02
TIR1	1	T1	1	1.08E-01	9.22E-02	2.80E+00	3.14E-03	3.41E-02
TIR1	1	T2	1	1.08E-01	9.22E-02	4.92E+00	3.14E-03	1.10E-02
TIR1	6	FL	1	1.08E-01	9.22E-02	6.89E+00	3.14E-03	3.59E-02
TIR1	6	T1	1	1.08E-01	9.22E-02	5.53E+00	3.14E-03	3.22E-02
TIR1	6	T2	1	1.08E-01	9.22E-02	6.06E+00	3.14E-03	1.32E-02
TIR1	28	FL	1	1.08E-01	9.22E-02	5.81E+00	3.14E-03	1.70E-02
TIR1	28	T1	1	1.08E-01	9.22E-02	5.94E+00	3.14E-03	2.96E-02
TIR1	28	T2	1	1.08E-01	9.22E-02	7.22E+00	3.14E-03	3.16E-02
TIR1	28	T2V	1	1.08E-01	9.22E-02	8.39E+00	3.14E-03	6.79E-03
TIR1	1	FL	2	1.42E-01	1.72E-01	6.70E+00	3.19E-03	4.55E-02
TIR1	1	T1	2	1.42E-01	1.72E-01	2.82E+00	3.19E-03	4.44E-02
TIR1	1	T2	2	1.42E-01	1.72E-01	4.76E+00	3.19E-03	1.24E-02
TIR1	6	FL	2	1.42E-01	1.72E-01	7.73E+00	3.19E-03	4.62E-02
TIR1	6	T1	2	1.42E-01	1.72E-01	5.97E+00	3.19E-03	4.45E-02
TIR1	6	T2	2	1.42E-01	1.72E-01	6.57E+00	3.19E-03	1.81E-02
TIR1	28	FL	2	1.42E-01	1.72E-01	5.84E+00	3.19E-03	1.98E-02
TIR1	28	T1	2	1.42E-01	1.72E-01	5.99E+00	3.19E-03	3.50E-02
TIR1	28	T2	2	1.42E-01	1.72E-01	7.28E+00	3.19E-03	3.59E-02
TIR1	28	T2V	2	1.42E-01	1.72E-01	8.14E+00	3.19E-03	7.51E-03
AFB2	1	FL	1	1.49E-01	1.18E-01	7.13E+00	3.63E-03	9.16E-02
AFB2	1	T1	1	1.49E-01	1.18E-01	3.21E+00	3.63E-03	1.05E-01
AFB2	1	T2	1	1.49E-01	1.18E-01	4.91E+00	3.63E-03	2.35E-02
AFB2	6	FL	1	1.49E-01	1.18E-01	7.43E+00	3.63E-03	1.25E-01
AFB2	6	T1	1	1.49E-01	1.18E-01	6.03E+00	3.63E-03	1.82E-01
AFB2	6	T2	1	1.49E-01	1.18E-01	6.32E+00	3.63E-03	6.81E-02
AFB2	28	FL	1	1.49E-01	1.18E-01	6.21E+00	3.63E-03	4.02E-02
AFB2	28	T1	1	1.49E-01	1.18E-01	6.70E+00	3.63E-03	7.67E-02
AFB2	28	T2	1	1.49E-01	1.18E-01	7.84E+00	3.63E-03	7.03E-02
AFB2	28	T2V	1	1.49E-01	1.18E-01	8.97E+00	3.63E-03	1.97E-02
AFB2	1	FL	2	1.27E-01	8.77E-02	7.63E+00	3.25E-03	7.44E-02
AFB2	1	T1	2	1.27E-01	8.77E-02	3.15E+00	3.25E-03	8.17E-02
AFB2	1	T2	2	1.27E-01	8.77E-02	4.88E+00	3.25E-03	1.69E-02
AFB2	6	FL	2	1.27E-01	8.77E-02	7.14E+00	3.25E-03	1.30E-01
AFB2	6	T1	2	1.27E-01	8.77E-02	5.83E+00	3.25E-03	1.87E-01
AFB2	6	T2	2	1.27E-01	8.77E-02	6.10E+00	3.25E-03	7.32E-02
AFB2	28	FL	2	1.27E-01	8.77E-02	5.83E+00	3.25E-03	2.91E-02
AFB2	28	T1	2	1.27E-01	8.77E-02	6.68E+00	3.25E-03	5.88E-02
AFB2	28	T2	2	1.27E-01	8.77E-02	7.65E+00	3.25E-03	5.35E-02
AFB2	28	T2V	2	1.27E-01	8.77E-02	8.64E+00	3.25E-03	1.39E-02

Supplementary Table 7: Average, minimum and maximum values of the estimated parameters in Supplementary Tables 4 and 5.

	average	min (% of average)	max (% of average)
k_1	0.13	0.11 (82)	0.15 (138)
k_2	0.12	8.8E-2 (74)	0.17 (195)
k_3	6.98	2.47 (35)	11.6 (468)
k_4	3.3E-3	3.1E-3 (95)	3.6E-3 (116)
k_5	3.87E-2	2.2-3 (5.7)	0.11 (51)

Supplemental Table 8: Oligonucleotides used in this study

ORF	Forward primer	Reverse primer
IAA1	ATGGAAGTCACCAATGGGCTTAACCTTAAG	TCATAAGGCAGTAGGAGCTTCGGATCC
IAA2	ATGGCGTACGAGAAAGTCAACGAGCTTAAC	TCATAAGGAAGAGTCTAGAGCAGGAGCGTC
IAA3	ATGGATGAGTTTGTTAACCTCA	TTATCATACACCACAGCCTAAAC
IAA4	ATGGAAAAAGTTGATGTTTATGATGAGCTTGTTAACCTAAAG	TTAAAGACCACCACAACCTAAACCTTTAACTTCAGATC
IAA5	ATGGCGAATGAGAGTAATAATCTTGGACTCG	TCATCCTCTGTTACATGATCTCTTCATAATCCTTAACC
IAA6	ATGGCAAAGGAAGGTCTAGCACTCGAG	TTAATCTTGCTGGAGACCAAAACCAGTTG
IAA7	ATGATCGGCCAACTTATGAACCTCAAG	TCAAGATCTGTTCTTGCAGTACTTCTCCATTG
IAA8	ATGAGTTCTGGGAACGATAAGATAAAACAAGTCC	TCAAACCCGCTCTTTGTTCTTCGATTTC
IAA9	ATGTCCCCGGAAGAGGAGCTACAGAG	TTAAGCTCTCATCTTCGATTTCTCCATTGC
IAA10	ATGAATGGTTTGCAAGAAGTTTGTTCGTC	CTACTTACCTACTCCAGCTCCAATTGATGTCTTCATG
IAA11	ATGGAAGGCGGTTCCGCTAGTG	TCATAATATCATCTGAGCTTTACCAGTAGCCTCC
IAA12	ATGCGTGGTGTGTCAGAATTGGAG	CTAAACAGGGTTGTTTCTTTGTCTATCCTTCTGC
IAA13	ATGATTACTGAACTTGAGATGGGGAAAGGTG	CTAAACCGGCTGCTTTCGCTGTC
IAA14	ATGAACCTTAAGGAGACGG	TTATCATGATCTGTTCTTGAACTTC
IAA15	ATGTCACCGGAGGAATACGTTAGGGTTTG	CTATAATCCAATAGCATCTCCGGTTTTCATTAACCTC
IAA17	ATGATGGGCAGTGTCGAGCTGAATC	TCAAGCTCTGCTCTTGCACTTCTCCATC
IAA18	ATGGAGGGTTATTCAAGAAAC	TTATCATCTTCTCATTTTCTCTTGC
IAA19	ATGGAGAAGGAAGGACTC	TTATCACTCGTCTACTCCTCTAGG
IAA20	ATGGGAAGAGGGAGAAGTTCATCGTC	TCAGTAGTGGTAATTAGCTCTTGAAATCTTCAGTCTTCTC
IAA26	ATGGAAGGTTGTCCAAGAAACAGAGAAATC	TCAGTGCATCATCTTCTCTTGCTTACTGC
IAA27	ATGTCTGTATCTGTAGCAGCAGAGCATGATTACATAG	CTAGTTCCTGCTTCTGCACTTCTCCATCAC
IAA28	ATGGAAGAAGAAAAGAGATTGG	TTACTATTCCTTGCCATGTTTTC
IAA31	ATGGAGGTCTCTAACTCTTGTTCTTCATTTTCTTCATC	TTAATACCTCTCCGGTCTCGTGATCTTTAGTCTTC
IAA32	ATGGACCCAAACACACCTGCAGAC	TTAAAAGGGAAGAAGAGCATCGTTTCTTCTTG
TIR1	ATGCAGAAGCGAATAGCCTTGTCG	TTATAATCCGTTAGTAGTAATGATTTGCCTGGAAAACC
AFB2	ATGAATTATTTCCCAGATGAAGTAATAGAGCATGTATTC	TTAGAGAATCCACACAAATGGCGG
mTIR1	ATGGTCTTCATCGGGAACTGCTACGC	TTATAATCCGTTAGTAGTAATGATTTGCCTGGAAAACC
AFB1	ATGGGTCTCCGATTCCCACCTAAG	TTACTTTATGGCTAGATGTGAAACTCCATTCTCAG
AFB3	ATGAATTATTTCCCAGACGAGGTTATAGAGCAC	CTAAAGAATCCTAACATATGGTGGTGCATCTTTTC

*all forward primers had AAAAAGCAGGCTTCAAA appended to the 5' end

**all reverse primers had AGAAAGCTGGGTG appended to the 5' end

Sequencing Primers

All Coding - M13F	GTAAAACGACGGCCAGT
All Coding - M13R	GGAAACAGCTATGACCATG
TIR1, mTIR1 (bp 663-682)	TGTTCCACTTGAAAAATTGG
TIR1, mTIR1 (bp 751-734)	GTCGCACTTCTGCAGTGT
AFB2	CTGATGGTCTTGCCTCTATTG
AFB1 (bp 478-501)	CGAGAGTGTATTGTTGAAGATTTA
AFB3 (bp 404-424)	GTGAAGGGTTTACCACTGATG

Primers used for Gibson Assembly of truncations

Template or construct	Forward	Reverse
YFP-IAA17.T1-NLS	ATCACTCTCGGCATGGACGAG	AGCGTGACATAACTAATTACATGACATCGATT
pGP4GY	GTTATGTCACGCTTACATTCACGCCC	GAGAGTGATCCCGGCGGC
IAA1.FL	TGCCGGGCCCATGGAAGTCACCAATGGGCTTAACC	GGGGGCGCCAGCACCTAAGGCAGTAGGAGCTTCGGATCCT
pGP4GY:IAA1.FL	GGTGCTGGCGCCCCCA	CCATTGGTGACTTCCATGGGCCCGGCACCC
IAA1.T1	TGCCGGGCCCATGGAAGTCACCAATGGGCTTAACC	AGCACCACTCACGTTTTTGTTGTTGTTGTTCTTACG
pGP4GY:IAA1.T1	AACAAAAACGTGAGTGGTGCTGGCGCCCC	CCATTGGTGACTTCCATGGGCCCGGCACCC
IAA1.T2	CCGGGCCCAACGACTCAACAGAAGAATCTGCTCCTC	AGCACCACTCACGTTTTTGTTGTTGTTGTTCTTACG
pGP4GY:IAA1.T2	AACAAAAACGTGAGTGGTGCTGGCGCCCC	TCTTCTGTTGAGTCGTTGGGCCCGGCACCC
IAA6.FL	TGCCGGGCCCATGGCAAAGGAAGGTCTAGCACTCG	GGGGGCGCCAGCACCATCTTGCTGGAGACCAAAACCAGTT
pGP4GY:IAA6.FL	GGTGCTGGCGCCCCCA	AGACCTTCCTTTGCCATGGGCCCGGCACCC
IAA6.T1	TGCCGGGCCCATGGCAAAGGAAGGTCTAGCACTCG	CCAGCACCGCCTATAGCTTTCGATGCTTCCTCATTG
pGP4GY:IAA6.T1	TCGAAAGCTATAGGCGGTGCTGGCGCCCC	AGACCTTCCTTTGCCATGGGCCCGGCACCC
IAA6.T2	TGCCGGGCCCGAATCACTGCCGGTTGTGAAGAGTC	CCAGCACCGCCTATAGCTTTCGATGCTTCCTCATTG
pGP4GY:IAA6T2	TCGAAAGCTATAGGCGGTGCTGGCGCCCC	ACAACCGGCAGTGATTCGGGCCCGGCACCC
IAA28.FL	GGCCCATGGAAGAAGAAAAGAGATTGGAGCTAAGGC	GGGGGCGCCAGCACCTTCCTTGCCATGTTTTCTAGGTGAGA
pGP4GY:IAA28.FL	GGTGCTGGCGCCCCCA	CTCTTTTCTTCTTCCATGGGCCCGGCACCC
IAA28.T1	GGCCCATGGAAGAAGAAAAGAGATTGGAGCTAAGGC	GCACCCAATTCCTTCTCTTCATCACTCTCCTTCTTC
pGP4GY:IAA28.T1	GAAGAGAAGGAATTGGGTGCTGGCGCCCC	CTCTTTTCTTCTTCCATGGGCCCGGCACCC
IAA28.T2	GTGCCGGGCCCAGGGTTGAGGTAGCTCCAGTGGTG	GCACCCAATTCCTTCTCTTCATCACTCTCCTTCTTC
pGP4GY:IAA28.T2	GAAGAGAAGGAATTGGGTGCTGGCGCCCC	GGAGCTACCTCAACCCTGGGCCCGGCACCC
IAA28.T2V	TGCCGGGCCCAAACAAAAAAGCTCGACCAAAGAAACA	GCGCCAGCACCGTTTCTCCGGGATGATCTCACCG
pGP4GY:IAA28.T2V	ATCATCCCGGAGAAACGGTGCTGGCGCCCC	GTCGAGCTTTTTTGTTTGGGCCCGGCACCC

Primers used for Gibson Assembly of the plant expression vector

IAA28.T2:DII-VENUS	TGTACAAAAAAGCAGGCTATGAGGGTTGAGGTAGCTCCAGTGG	GCAGCTGCCGCACAATTCCTTCTCTTCATCACTCTCCTT
DII-VENUS	TGCGGCAGCTGCGACCC	CATAGCCTGCTTTTTTGTACAAACTTGACTAGTGG

*primer names = annealing template sequence name:overlap for homologous assembly

**undelined regions anneal to the template, while the non-underlined are the additional sequence for homologous assembly

Supplementary Table 9: Yeast strains used in this study

Strain Name	Relevant Genotype
W303-1A	*MAT***a** *leu2-3,112 trp1-1 can1-100 ura3-1 ade2-1 his3-11,15*
W303-1B	*MATα leu2-3,112 trp1-1 can1-100 ura3-1 ade2-1 his3-11,15*
TIR1|IAA1	*MAT***a***/MATα LEU2:pGPD-TIR1/leu2-3,112 trp1-1/TRP1:pGPD-YFP-IAA1*
TIR1|IAA2	*MAT***a***/MATα LEU2:pGPD-TIR1/leu2-3,112 trp1-1/TRP1:pGPD-YFP-IAA2*
TIR1|IAA3	*MAT***a***/MATα LEU2:pGPD-TIR1/leu2-3,112 trp1-1/TRP1:pGPD-YFP-IAA3*
TIR1|IAA4	*MAT***a***/MATα LEU2:pGPD-TIR1/leu2-3,112 trp1-1/TRP1:pGPD-YFP-IAA4*
TIR1|IAA5	*MAT***a***/MATα LEU2:pGPD-TIR1/leu2-3,112 trp1-1/TRP1:pGPD-YFP-IAA5*
TIR1|IAA6	*MAT***a***/MATα LEU2:pGPD-TIR1/leu2-3,112 trp1-1/TRP1:pGPD-YFP-IAA6*
TIR1|IAA7	*MAT***a***/MATα LEU2:pGPD-TIR1/leu2-3,112 trp1-1/TRP1:pGPD-YFP-IAA7*
TIR1|IAA8	*MAT***a***/MATα LEU2:pGPD-TIR1/leu2-3,112 trp1-1/TRP1:pGPD-YFP-IAA8*
TIR1|IAA9	*MAT***a***/MATα LEU2:pGPD-TIR1/leu2-3,112 trp1-1/TRP1:pGPD-YFP-IAA9*
TIR1|IAA10	*MAT***a***/MATα LEU2:pGPD-TIR1/leu2-3,112 trp1-1/TRP1:pGPD-YFP-IAA10*
TIR1|IAA11	*MAT***a***/MATα LEU2:pGPD-TIR1/leu2-3,112 trp1-1/TRP1:pGPD-YFP-IAA11*
TIR1|IAA12	*MAT***a***/MATα LEU2:pGPD-TIR1/leu2-3,112 trp1-1/TRP1:pGPD-YFP-IAA12*
TIR1|IAA13	*MAT***a***/MATα LEU2:pGPD-TIR1/leu2-3,112 trp1-1/TRP1:pGPD-YFP-IAA13*
TIR1|IAA14	*MAT***a***/MATα LEU2:pGPD-TIR1/leu2-3,112 trp1-1/TRP1:pGPD-YFP-IAA14*
TIR1|IAA15	*MAT***a***/MATα LEU2:pGPD-TIR1/leu2-3,112 trp1-1/TRP1:pGPD-YFP-IAA15*
TIR1|IAA17	*MAT***a***/MATα LEU2:pGPD-TIR1/leu2-3,112 trp1-1/TRP1:pGPD-YFP-IAA17*
TIR1|IAA18	*MAT***a***/MATα LEU2:pGPD-TIR1/leu2-3,112 trp1-1/TRP1:pGPD-YFP-IAA18*
TIR1|IAA19	*MAT***a***/MATα LEU2:pGPD-TIR1/leu2-3,112 trp1-1/TRP1:pGPD-YFP-IAA19*
TIR1|IAA20	*MAT***a***/MATα LEU2:pGPD-TIR1/leu2-3,112 trp1-1/TRP1:pGPD-YFP-IAA20*
TIR1|IAA26	*MAT***a***/MATα LEU2:pGPD-TIR1/leu2-3,112 trp1-1/TRP1:pGPD-YFP-IAA26*
TIR1|IAA27	*MAT***a***/MATα LEU2:pGPD-TIR1/leu2-3,112 trp1-1/TRP1:pGPD-YFP-IAA27*
TIR1|IAA28	*MAT***a***/MATα LEU2:pGPD-TIR1/leu2-3,112 trp1-1/TRP1:pGPD-YFP-IAA28*
TIR1|IAA29	*MAT***a***/MATα LEU2:pGPD-TIR1/leu2-3,112 trp1-1/TRP1:pGPD-YFP-IAA29*
TIR1|IAA31	*MAT***a***/MATα LEU2:pGPD-TIR1/leu2-3,112 trp1-1/TRP1:pGPD-YFP-IAA31*
TIR1|IAA32	*MAT***a***/MATα LEU2:pGPD-TIR1/leu2-3,112 trp1-1/TRP1:pGPD-YFP-IAA32*
AFB2|IAA1	*MAT***a***/MATα LEU2:pGPD-AFB2/leu2-3,112 trp1-1/TRP1:pGPD-YFP-IAA1*

Strain Name	Relevant Genotype
AFB2|IAA2	*MAT**a**/MATα LEU2:pGPD-AFB2/leu2-3,112 trp1-1/TRP1:pGPD-YFP-IAA2*
AFB2|IAA3	*MAT**a**/MATα LEU2:pGPD-AFB2/leu2-3,112 trp1-1/TRP1:pGPD-YFP-IAA3*
AFB2|IAA4	*MAT**a**/MATα LEU2:pGPD-AFB2/leu2-3,112 trp1-1/TRP1:pGPD-YFP-IAA4*
AFB2|IAA5	*MAT**a**/MATα LEU2:pGPD-AFB2/leu2-3,112 trp1-1/TRP1:pGPD-YFP-IAA5*
AFB2|IAA6	*MAT**a**/MATα LEU2:pGPD-AFB2/leu2-3,112 trp1-1/TRP1:pGPD-YFP-IAA6*
AFB2|IAA7	*MAT**a**/MATα LEU2:pGPD-AFB2/leu2-3,112 trp1-1/TRP1:pGPD-YFP-IAA7*
AFB2|IAA8	*MAT**a**/MATα LEU2:pGPD-AFB2/leu2-3,112 trp1-1/TRP1:pGPD-YFP-IAA8*
AFB2|IAA9	*MAT**a**/MATα LEU2:pGPD-AFB2/leu2-3,112 trp1-1/TRP1:pGPD-YFP-IAA9*
AFB2|IAA10	*MAT**a**/MATα LEU2:pGPD-AFB2/leu2-3,112 trp1-1/TRP1:pGPD-YFP-IAA10*
AFB2|IAA11	*MAT**a**/MATα LEU2:pGPD-AFB2/leu2-3,112 trp1-1/TRP1:pGPD-YFP-IAA11*
AFB2|IAA12	*MAT**a**/MATα LEU2:pGPD-AFB2/leu2-3,112 trp1-1/TRP1:pGPD-YFP-IAA12*
AFB2|IAA13	*MAT**a**/MATα LEU2:pGPD-AFB2/leu2-3,112 trp1-1/TRP1:pGPD-YFP-IAA13*
AFB2|IAA14	*MAT**a**/MATα LEU2:pGPD-AFB2/leu2-3,112 trp1-1/TRP1:pGPD-YFP-IAA14*
AFB2|IAA15	*MAT**a**/MATα LEU2:pGPD-AFB2/leu2-3,112 trp1-1/TRP1:pGPD-YFP-IAA15*
AFB2|IAA17	*MAT**a**/MATα LEU2:pGPD-AFB2/leu2-3,112 trp1-1/TRP1:pGPD-YFP-IAA17*
AFB2|IAA18	*MAT**a**/MATα LEU2:pGPD-AFB2/leu2-3,112 trp1-1/TRP1:pGPD-YFP-IAA18*
AFB2|IAA19	*MAT**a**/MATα LEU2:pGPD-AFB2/leu2-3,112 trp1-1/TRP1:pGPD-YFP-IAA19*
AFB2|IAA20	*MAT**a**/MATα LEU2:pGPD-AFB2/leu2-3,112 trp1-1/TRP1:pGPD-YFP-IAA20*
AFB2|IAA26	*MAT**a**/MATα LEU2:pGPD-AFB2/leu2-3,112 trp1-1/TRP1:pGPD-YFP-IAA26*
AFB2|IAA27	*MAT**a**/MATα LEU2:pGPD-AFB2/leu2-3,112 trp1-1/TRP1:pGPD-YFP-IAA27*
AFB2|IAA28	*MAT**a**/MATα LEU2:pGPD-AFB2/leu2-3,112 trp1-1/TRP1:pGPD-YFP-IAA28*
AFB2|IAA29	*MAT**a**/MATα LEU2:pGPD-AFB2/leu2-3,112 trp1-1/TRP1:pGPD-YFP-IAA29*
AFB2|IAA31	*MAT**a**/MATα LEU2:pGPD-AFB2/leu2-3,112 trp1-1/TRP1:pGPD-YFP-IAA31*
AFB2|IAA32	*MAT**a**/MATα LEU2:pGPD-AFB2/leu2-3,112 trp1-1/TRP1:pGPD-YFP-IAA32*
TIR1|IAA1.FL-NLS	*MAT**a**/MATα LEU2:pGPD-TIR1/leu2-3,112 trp1-1/TRP1:pGPD-YFP-IAA1-NLS*
TIR1|IAA1.T1-NLS	*MAT**a**/MATα LEU2:pGPD-TIR1/leu2-3,112 trp1-1/TRP1:pGPD-YFP-IAA1.T1-NLS*
TIR1|IAA1.T2-NLS	*MAT**a**/MATα LEU2:pGPD-TIR1/leu2-3,112 trp1-1/TRP1:pGPD-YFP-IAA1.T2-NLS*
TIR1|IAA6.FL-NLS	*MAT**a**/MATα LEU2:pGPD-TIR1/leu2-3,112 trp1-1/TRP1:pGPD-YFP-IAA6-NLS*
TIR1|IAA6.T1-NLS	*MAT**a**/MATα LEU2:pGPD-TIR1/leu2-3,112 trp1-1/TRP1:pGPD-YFP-IAA6.T1-NLS*
TIR1|IAA6.T2-NLS	*MAT**a**/MATα LEU2:pGPD-TIR1/leu2-3,112 trp1-1/TRP1:pGPD-YFP-IAA6.T2-NLS*

Strain Name	**Relevant Genotype**
TIR1|IAA28.FL-NLS	*MAT***a***/MATα LEU2:pGPD-TIR1/leu2-3,112 trp1-1/TRP1:pGPD-YFP-IAA28-NLS*
TIR1|IAA28.T1-NLS	*MAT***a***/MATα LEU2:pGPD-TIR1/leu2-3,112 trp1-1/TRP1:pGPD-YFP-IAA28.T1-NLS*
TIR1|IAA28.T2-NLS	*MAT***a***/MATα LEU2:pGPD-TIR1/leu2-3,112 trp1-1/TRP1:pGPD-YFP-IAA28.T2-NLS*
TIR1|IAA28.T2V-NLS	*MAT***a***/MATα LEU2:pGPD-TIR1/leu2-3,112 trp1-1/TRP1:pGPD-YFP-IAA28.T2V-NLS*
AFB2|IAA1.FL-NLS	*MAT***a***/MATα LEU2:pGPD-AFB2/leu2-3,112 trp1-1/TRP1:pGPD-YFP-IAA1-NLS*
AFB2|IAA1.T1-NLS	*MAT***a***/MATα LEU2:pGPD-AFB2/leu2-3,112 trp1-1/TRP1:pGPD-YFP-IAA1.T1-NLS*
AFB2|IAA1.T2-NLS	*MAT***a***/MATα LEU2:pGPD-AFB2/leu2-3,112 trp1-1/TRP1:pGPD-YFP-IAA1.T2-NLS*
AFB2|IAA6.FL-NLS	*MAT***a***/MATα LEU2:pGPD-AFB2/leu2-3,112 trp1-1/TRP1:pGPD-YFP-IAA6-NLS*
AFB2|IAA6.T1-NLS	*MAT***a***/MATα LEU2:pGPD-AFB2/leu2-3,112 trp1-1/TRP1:pGPD-YFP-IAA6.T1-NLS*
AFB2|IAA6.T2-NLS	*MAT***a***/MATα LEU2:pGPD-AFB2/leu2-3,112 trp1-1/TRP1:pGPD-YFP-IAA6.T2-NLS*
AFB2|IAA28.FL-NLS	*MAT***a***/MATα LEU2:pGPD-AFB2/leu2-3,112 trp1-1/TRP1:pGPD-YFP-IAA28-NLS*
AFB2|IAA28.T1-NLS	*MAT***a***/MATα LEU2:pGPD-AFB2/leu2-3,112 trp1-1/TRP1:pGPD-YFP-IAA28.T1-NLS*
AFB2|IAA28.T2-NLS	*MAT***a***/MATα LEU2:pGPD-AFB2/leu2-3,112 trp1-1/TRP1:pGPD-YFP-IAA28.T2-NLS*
AFB2|IAA28.T2V-NLS	*MAT***a***/MATα LEU2:pGPD-AFB2/leu2-3,112 trp1-1/TRP1:pGPD-YFP-IAA28.T2V-NLS*

References

[1] Caldern-Villalobos LIA, Lee S, Oliveira CD, Ivetac A, Brandt W, Armitage L, Sheard LB, Tan X, Parry G, Mao H, Zheng N, Napier R, Kepinski S & Estelle M (2012) A combinatorial TIR1/AFB-Aux/IAA co-receptor system for differential sensing of auxin. Nat Chem Biol 8: 477-485

[2] Brunoud G, Wells DM, Oliva M, Larrieu A, Mirabet V, Burrow AH, Beeckman T, Kepinski S, Traas J, Bennett MJ & Vernoux T (2012) A novel sensor to map auxin response and distribution at high spatio-temporal resolution. Nature 482: 103-6

[3] Gibson DG, Young L, Chuang R-Y, Venter JC, Hutchison CA & Smith HO (2009) Enzymatic assembly of DNA molecules up to several hundred kilobases. Nat Methods 6: 343-345

[4] Dreher KA, Brown J, Saw RE & Callis J (2006) The Arabidopsis Aux / IAA Protein Family Has Diversified in Degradation and Auxin Responsiveness. Plant Cell 18: 699-714

[5] Ramos J, Zenser N, Leyser O & Callis J (2001) Rapid degradation of auxin/indoleacetic acid proteins requires conserved amino acids of domain II and is proteasome dependent. Plant Cell 13: 2349-2360

[6] Ouellet F, Overvoorde PJ & Theologis A (2001) IAA17/AXR3: biochemical insight into an auxin mutant phenotype. Plant Cell. 13: 829-41.

[7] Gray WM, Kepinski S, Rouse D, Leyser O & Estelle M (2001) Auxin regulates SCF(TIR1)-dependent degradation of AUX/IAA proteins. Nature 414: 271-6.